Distinct Waves from the Hemogenic Endothelium Give Rise to Layered Lymphoid Tissue Inducer Cell Ontogeny

Cell Reports

Article

Distinct Waves from the Hemogenic Endothelium Give Rise to Layered Lymphoid Tissue Inducer Cell Ontogeny

Graphical Abstract

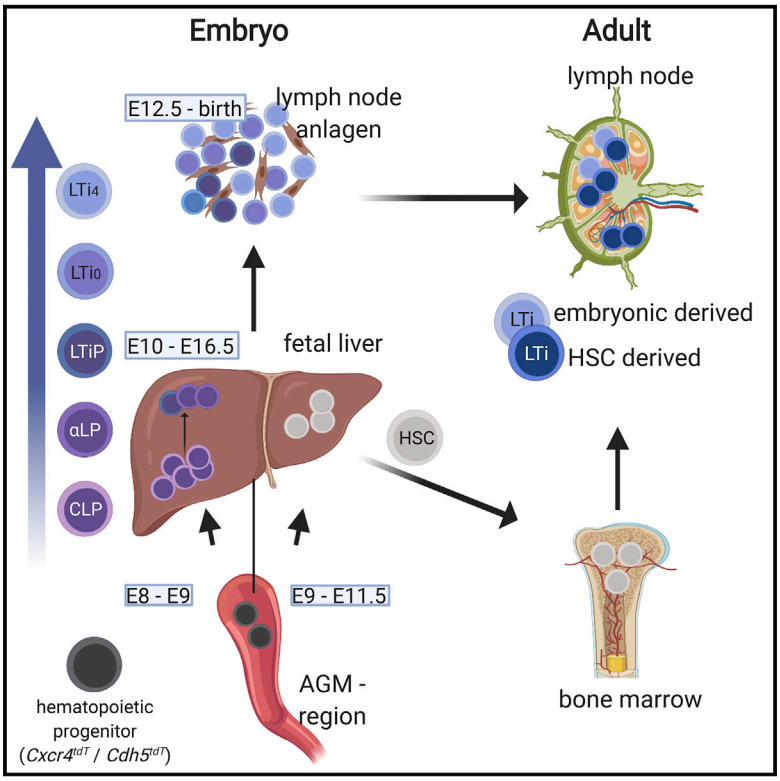

Highlights

- LTi progenitors originate from early embryonic hemogenic endothelium, excluding yolk sac
- The fetal liver harbors proliferating LTi precursor populations
- LTi maturation occurs in the periphery into two LTi_4 populations
- Embryonic LTi are replaced by HSC-derived LTi cells in adults

Authors

Milesa Simic, Iris Manosalva, Lionel Spinelli, ..., Ralf Stumm, Rachel Golub, Serge A. van de Pavert

Correspondence

vandepavert@ciml.univ-mrs.fr

In Brief

Simic et al. present a detailed view of LTi ontogeny. Hemogenic progenitors appear specifically in early embryonic hemogenic endothelium and via proliferating precursor populations in the fetal liver and ultimately differentiate into two mature LTi_4 populations within the embryonic periphery. In adults, embryonic LTi cells are replaced by HSC-derived LTi cells.

Simic et al., 2020, Cell Reports *32*, 108004
August 11, 2020
https://doi.org/10.1016/j.celrep.2020.108004

CellPress

Cell Reports

CellPress
OPEN ACCESS

Article

Distinct Waves from the Hemogenic Endothelium Give Rise to Layered Lymphoid Tissue Inducer Cell Ontogeny

Milesa Simic,[1] Iris Manosalva,[1] Lionel Spinelli,[1] Rebecca Gentek,[1,4] Raheleh R. Shayan,[1] Carole Siret,[1] Mathilde Girard-Madoux,[1] Shuaiwei Wang,[1] Lauriane de Fabritus,[1] Janneke Verschoor,[1] Yann M. Kerdiles,[1] Marc Bajenoff,[1] Ralf Stumm,[2] Rachel Golub,[3] and Serge A. van de Pavert[1,5,*]

[1]Aix-Marseille Université, Centre National de la Recherche Scientifique (CNRS), Institut National de la Santé et de la Recherche Médicale (INSERM), Centre d'Immunologie de Marseille-Luminy (CIML), 13288 Marseille, France
[2]Institute of Pharmacology and Toxicology, Jena University Hospital, Friedrich Schiller University Jena, 07747 Jena, Germany
[3]Institut Pasteur, Immunology Department, Lymphopoiesis Unit, INSERM U668, University Paris Diderot, Paris, France
[4]Present address: Centre for Inflammation Research (CIR), Institute of Regeneration and Repair, University of Edinburgh, Edinburgh, UK
[5]Lead Contact
*Correspondence: vandepavert@ciml.univ-mrs.fr
https://doi.org/10.1016/j.celrep.2020.108004

SUMMARY

During embryogenesis, lymphoid tissue inducer (LTi) cells are essential for lymph node organogenesis. These cells are part of the innate lymphoid cell (ILC) family. Although their earliest embryonic hematopoietic origin is unclear, other innate immune cells have been shown to be derived from early hemogenic endothelium in the yolk sac as well as the aorta-gonad-mesonephros. A proper model to discriminate between these locations was unavailable. In this study, using a *Cxcr4-CreERT2* lineage tracing model, we identify a major contribution from embryonic hemogenic endothelium, but not the yolk sac, toward LTi progenitors. Conversely, embryonic LTi cells are replaced by hematopoietic stem cell-derived cells in adults. We further show that, in the fetal liver, common lymphoid progenitors differentiate into highly dynamic alpha-lymphoid precursor cells that, at this embryonic stage, preferentially mature into LTi precursors and establish their functional LTi cell identity only after reaching the periphery.

INTRODUCTION

The innate lymphoid cell (ILC) family was recognized about 10 years ago (Vivier et al., 2018) and is considered the innate counterpart of T lymphocytes but without antigen receptor rearrangement. ILC type 3 (ILC3) is characterized by expression of the nuclear transcription factor retinoic acid receptor-related orphan receptor variant γt (RORγt), which is encoded by the gene *Rorc* and is mostly associated with gut and skin immunity (Rankin et al., 2016). Initially characterized as an ILC3 subtype, lymphoid tissue inducer (LTi) cells are the first ILC family members observed during life and are critically involved in lymph node (LN) formation within the embryo (van de Pavert and Mebius, 2010; van de Pavert and Vivier, 2016; van de Pavert et al., 2014). The earliest described LTi progenitor is the common lymphoid progenitor (CLP) stage, which, through the alpha-lymphoid precursor (αLP) stage, differentiates toward LTi precursors (LTiPs) and, subsequently, into RORγt$^+$ LTi_0 cells (Chea et al., 2016; Ishizuka et al., 2016b, 2016a; van de Pavert et al., 2014). LTi_4 cells are the final stage in LTi ontogeny and additionally express CD4, TNF-related activation-induced cytokine (TRANCE, also known as tumor necrosis factor ligand superfamily member 11 [TNFSF11] or receptor activator of nuclear factor kappa B ligand [RANKL]), and lymphotoxin-αβ (van de Pavert et al., 2014) to facilitate interaction with mesenchymal lymphoid tissue organizer (LTo) cells within LN anlagen via the lymphotoxin receptor pathway. This amplifies expression of chemokines, cytokines, and retention molecules from LTo cells to attract and retain more LTi cells (van de Pavert and Mebius, 2010; Vondenhoff et al., 2009). LN formation starts with clustering of LTi cells with LTo cells, initially without lymphotoxin signaling, at embryonic day 12.5 (E12.5) (van de Pavert et al., 2009; Veiga-Fernandes et al., 2007). After E14.5, a dramatic increase in LN anlagen size can be observed because of activation of the lymphotoxin signaling pathway (van de Pavert and Mebius, 2010).

The hematopoietic source of CLPs is currently unknown. The earliest hematopoietic cells are generated by special endothelial cells, called hemogenic endothelial cells, located in the extra-embryonic yolk sac (YS) or in embryonic regions, of which the aorta-gonad-mesonephros (AGM) region is the most-studied region, that transition into hematopoietic progenitor cells (Boisset et al., 2010; Lancrin et al., 2009). It has been shown that the first hematopoietic progenitors appear from the YS and include, e.g., microglia, erythroid-myeloid progenitors, neutrophils, and mast cells, whereas later lineages and hematopoietic stem cells (HSCs) appear from the AGM at later time points (Gentek et al., 2018; Mass et al.,

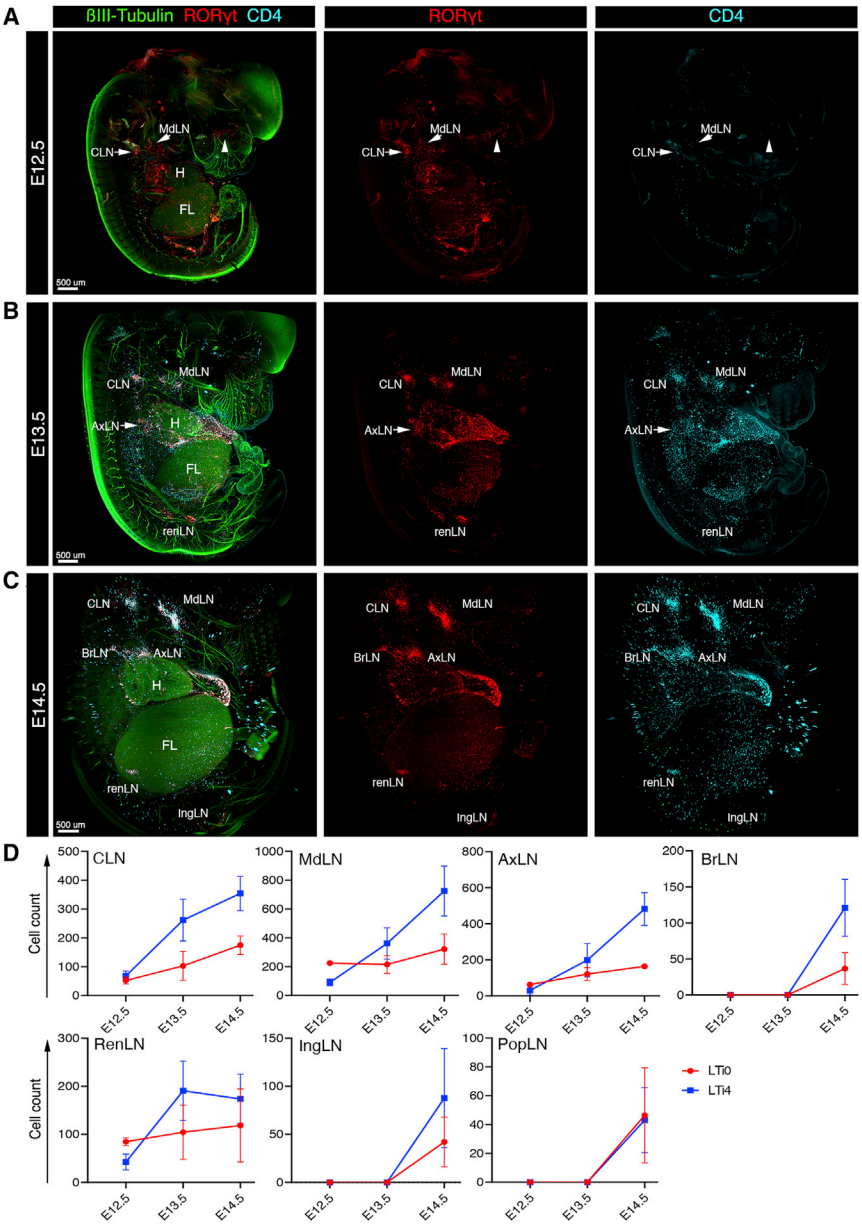

Figure 1. Quantification of LN Formation in Whole-Mount E12.5–E14.5 Embryos

Whole *RORγt*^{eGFP} embryos were analyzed at E12.5–E14.5 by light sheet microscopy.

(A–C) Projections of the light sheet analysis of RORγt$^+$ (red) and CD4$^+$ (cyan) cells in the different LN anlagen from the right half of the whole mount *RORγt*^{eGFP} embryos at (A) E12.5, (B) E13.5, and (C) E14.5. For orientation purposes, neurons were visualized by βIII-tubulin (green). Using the spot-function tool in Imaris, we annotated these cells as spots, which were subsequently quantified. There is staining within the sac around the heart, most likely not LTi cells because of their size. Embryos are orientated with the head up, dorsal side at the left, and ventral to the right. CLN, cervical lymph node; MdLN, mandibular LN; BrLN, brachial LN; AxLN, axillary LN; RenLN, renal LN; IngLN, inguinal LN anlagen. Scale bars, 500 μm.

(D) Quantification of LTi$_0$ and LTi$_4$ cells within the LN anlagen over time in embryonic gestation, based on the number of CD4$^+$ (LTi$_4$) spots and RORγt$^+$ minus the CD4$^+$ spots (LTi$_0$).

Data shown are averages ± SD; all data are based on at least 2 independent experiments. See also Figures S1A and S1B and Videos S1, S2, and S3.

2016; McGrath et al., 2015a, 2015b; Yoder, 2014). Subsequently, most hematopoietic progenitors migrate to the fetal liver (FL) to expand and differentiate toward precursors stages of their respective lineages. Coming from the FL, HSCs migrate via the embryonic spleen to colonize the bone marrow around E16.5 and, during adulthood, are responsible for continuous replacement of definitive hematopoietic lineages (Gao et al., 2018). Although ILC progenitors have been shown to be generated from HSCs in the bone marrow, formation of LTi cells from HSCs has not yet been shown (Seillet et al., 2016; Walker et al., 2019; Xu et al., 2019). When LTi progenitors differentiate from the hemogenic endothelium and whether they would appear concomitantly with HSCs is still unknown. In addition, LTi cell differentiation pathways occurring in the FL and at which stage in their ontogeny LTi cells colonize the embryonic periphery remains unclear.

In this study, we were able to discriminate between the appearance of hematopoietic progenitors from the YS and early embryonic hematopoietic regions using a lineage tracing model. Specifically, we show the complete ontogeny and respective locations of LTi cells, from their first appearance at the hemogenic endothelium to formation of LNs in the embryo. Multiple experimental approaches collectively show the importance of the FL in the expansion and differentiation of LTiPs before LTi cells colonize the embryonic periphery. Finally, we demonstrate that embryonic LTi cells are replaced in adult lymphoid tissues by HSC-derived cells.

RESULTS

Visualization of LN Formation in Whole-Mount Embryos

To comprehensively study embryonic LN formation, we first used whole-mount 3D immunofluorescence on E11.5–E14.5 *RORγt*^{EGFP} embryos. We separately quantified LTi$_0$ and LTi$_4$ populations within all LN anlagen using the spotfunction tool in Imaris (Figures 1A–1D, S1A, and S1B; Videos S1, S2, and S3). Although we did not observe any LTi cells in E11.5 *RORγt*^{eGFP} embryos (data not shown), clusters of LTi$_0$ cells (RORγt$^+$ cells) and LTi$_4$ (RORγt$^+$CD4$^+$) cells started to appear at E12.5 (Figures

1A and S1A; Video S1). At this stage, small LTi_0 clusters as well as the presumptive cervical LN (CLN) anlagen and mandibular LN (MdLN) anlagen were located very close to each other in the cervical region. A second cluster could also be observed in the axillary region but not yet the separate brachial LN (BrLN) anlagen and axillary LN (AxLN) anlagen. Finally, a third cluster was present near the mesonephros, which we identified as the renal LNs (RenLNs). Interestingly, we found numerous $ROR\gamma t^{+}CD4^{-}$ cells within the nasal cavity (arrowhead in Figure 1A), possibly involved in formation of nasal-associated lymphoid tissues during later gestation. At E13.5 (Figures 1B and S1A; Video S2), LTi_0 and LTi_4 cells further accumulate and allow identification of the cLN and MdLN anlagen within the cervical region. However, despite the presence of an LTi cluster close to the skin in the axillary region, the AxLN and BrLN anlagen still could not be clearly discriminated. Also, because of scattered $ROR\gamma t^{+}$ and $CD4^{+}$ cells within the gut and spleen, it was not possible to discriminate between stretched mesenteric LN anlagen and intestinal ILCs. By E14.5 (Figures 1C and S1A; Video S3), most peripheral LN anlagen (CLNs, MdLNs, AxLNs, BrLNs, RenLNs, and inguinal LNs [IngLNs]) could be identified and counted using Imaris, whereas the popliteal LNs (PopLNs) were still very small (Figures 1C, 1D, S1A, and S1B).

LTi_0 and LTi_4 Cells Are Mainly Present within the Periphery

After quantification of the LTi_0 and LTi_4 cells that formed the LN anlagen within the periphery, we set out to quantify all populations described within the LTi ontogeny. We used $ROR\gamma t^{EGFP}$ embryos between E11.5 and E14.5 and analyzed these populations within the FL and embryonic periphery using flow cytometry. Because it was not possible to distinguish between αLP and LTiP in flow cytometry, we used the annotation LTiP for this stage for all of our flow cytometry data. We observed that all populations increased during embryonic stages (Figures 2A–2C and numbers in Figure S2B). Further, although the CLPs were mostly present in the FL, similar numbers of LTiP cells were recovered from the periphery and the FL, and LTi_0 and LTi_4 cells were detected primarily within the periphery.

The marked increase in LTi cells between E13.5 and E14.5 suggested increased cell influx and/or increased local proliferation. To understand this phenomenon, we performed a 5-ethynyl-2′-deoxyuridine (EdU) assay at E13.5. We observed that proliferation was similar in CLPs obtained from the FL and periphery (Figure 2D). The most proliferative cells were LTiP cells obtained from the FL, whereas proliferation was lower in peripheral LTiP cells. LTi cells showed the lowest proliferation, especially in the periphery. These data suggest that the increase of LTi cells at E14.5 is primarily due to proliferation of CLP and especially LTiP cells in the FL and, thus, that the increase in LN anlagen was due to increased LTiP influx.

Transcriptional Expression Profiling of the LTi Ontogeny in FL versus the Periphery

To study whether there is a correlation in LTi ontogeny within the FL toward LTi cells in the periphery, we sort-purified the populations involved in LTi ontogeny from both tissues and compared their transcription expression profiles by bulk RNA sequencing. The populations isolated from the FL and periphery were CLP, LTiP, LTi_0 and LTi_4. In the principal-component analysis (PCA) comparison, the CLP and LTiP populations highly segregated against the LTi_0 and LTi_4 populations (Figures 3A and 3B), independent of tissue origin. The similarities in gene expression within the LTi_0 and LTi_4 populations were high, including ILC3-associated genes such as *Il22* and *Il17a* (highlighted in Figure 3B). Also, *Rxrg*, a retinoic acid receptor, was expressed by LTiP, LTi_0, and LTi_4 populations (highlighted in Figure 3B), suggesting that LTiP cells became responsive to retinoic acid, which has been shown to be required for the next step in differentiation (van de Pavert et al., 2014). We observed the largest segregation between the LTiP and LTi_0 populations (57% of observed variance; Figure 3C). The heatmap for these stages also combined all LTi_0 samples versus all LTiP samples, regardless of their origin (Figure 3D). These data suggest that differentiation between LTiP and LTi_0 induced the largest variation. The segregation between CLP and LTiP versus LTi_0 and LTi_4 cells, regardless of their origin, was also observed when the best loading genes of each axis were compared with all other populations in the correlation matrix (Figure 3E). The blue clusters indicate a positive correlation, which was observed in the LTiP/CLP stages versus the LTi_0/LTi_4 stages, independent of tissue origin. Many LTi cell-associated genes, such as *LTb*, *Cxcr6*, and *S1pr1* (Figure 3F), and transcription factors, such as *Rorc* and *Tcf7* (Figure S3C), were similarly upregulated in FL- and periphery-derived LTi cells. Also, other gene expression patterns across the differentiation stages, as shown in the evolution plots for cytokines (Figure S3D), tumor necrosis factor (TNF)-associated genes (Figure S3E), or Notch signaling-associated genes (Figure S3F), were almost similar in FL versus peripherally obtained LTi cells. In summary, the most distinguishing stage was between the LTiP and LTi_0 stage, when *Rorc* (RORγt) expression established a LTi phenotype. Based on the very low number of LTi_0 and LTi_4 cells within the FL (Figures 2A–2C), which had similar expression profiles as peripheral LTi cells, we propose that LTi_0 and LTi_4 cells differentiate in the periphery from LTiP cells.

Single-Cell Sequencing Revealed that CLPs Preferentially Differentiate into ILC3 and LTi Cells within the Periphery at E13.5

To better understand the steps involved in LTi differentiation within the embryonic periphery, we performed single-cell sequencing analysis on $CD45^{+}Lin^{-}F4/80^{-}Il7R\alpha^{+}$ cells obtained from E13.5 and E14.5 FL and embryonic periphery (for gating of the populations, see Figure S4). After normalization, quality control, and removal of clusters of residual macrophages (*Cx3cr1*), pre-mature B cells (*CD79a*), and mast cells (*Oms*) for analysis, we used 2,715 cells from E13.5 periphery, 2,978 cells from E14.5 periphery, 6,616 cells from E13.5 FL, and 2,034 cells from E14.5 FL. In the FL, about half of the cells were clustered because of genes associated with proliferation, indicating a switch between a proliferative state and differentiation at each stage (Figures S5B and S5D). Even though we excluded macrophages by *Cx3cr1* and pro-B cells by *CD79a*, we still observed some clearly separated clusters in the FL (9 and 13 at E13.5 and 10 and 11 at E14.5; Figure S5), which could be monocyte- or B cell-fated cells.

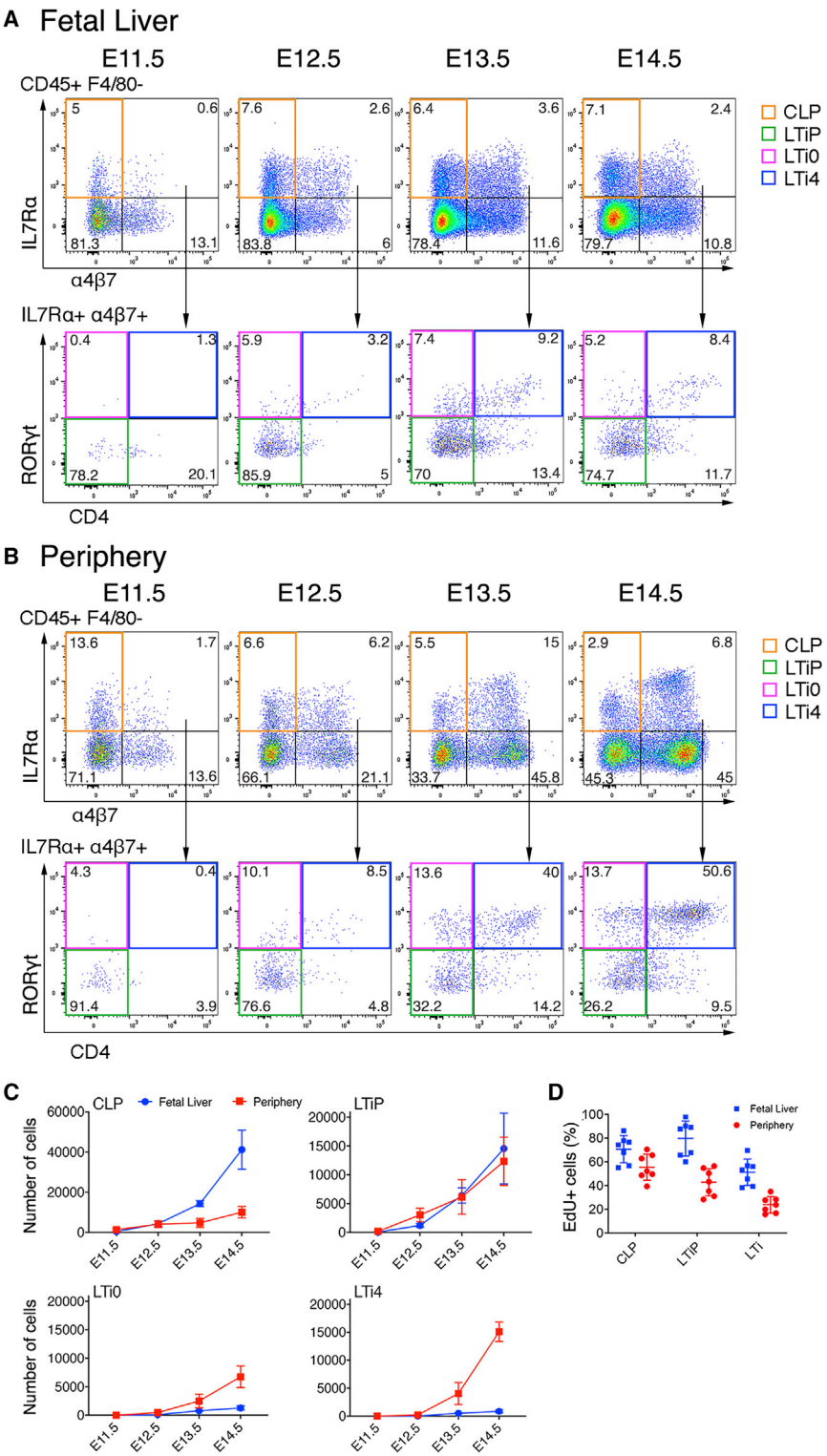

Figure 2. Analysis of the Populations in LTi Ontogeny

(A and B) Representative flow cytometry plots of LTi ontogeny at embryonic stages E11.5–E14.5 from *RORγt*^{eGFP} embryos in the FL (A) and embryonic periphery (B), enriched for the peripheral LN anlagen. CLPs are defined as CD45$^+$F4/80$^-$IL7Rα$^+$α$_4$β$_7^-$RORγt$^-$CD4$^-$ cells, LTiPs as CD45$^+$F4/80$^-$IL7Rα$^+$α$_4$β$_7^+$RORγt$^-$CD4$^-$ cells, LTi$_0$ as CD45$^+$F4/80$^-$IL7Rα$^+$α$_4$β$_7^+$RORγt$^+$CD4$^-$ cells, and LTi$_4$ as CD45$^+$F4/80$^-$IL7Rα$^+$α$_4$β$_7^+$RORγt$^+$CD4$^+$ cells. The numbers shown in the plots are average percentages for each population. For the gating strategy, see Figure S2A. Numbers are shown in the table in Figure S2B.

(C) Graphical representation showing the average cell counts ± SD of flow cytometry in time. Cell counts represent absolute cell numbers present in each tissue and were obtained by multiplying the percentage of the total for each cell subtype multiplied by the total number of cells counted before staining.

(D) Proliferation of the LTi populations within E13.5 *RORγt*^{eGFP} embryos in the FL and periphery by flow cytometry 2 h after EdU injection in a pregnant mouse. LTi cells are defined as CD45$^+$F4/80$^-$IL7Rα$^+$α$_4$β$_7^+$RORγt$^+$ and include LTi$_0$ and LTi$_4$. For the gating strategy, see Figure S2C.

Data shown are from at least two independent experiments and are shown as average ± SD. Single data points in (D) represent individual embryos.

Using flow cytometry, it was impossible to delineate αLPs from LTiPs (both being Il7Rα$^+$, α4β7$^+$RORγt$^-$; Figure 2). However, using single-cell sequencing, we were able to distinguish both populations separately in the FL as *Itga4*$^+$*Id2*$^+$*Cxcr5*$^-$ αLPs (clusters 1, 3, and 8 at E13.5 and clusters 2 and 5 at E14.5) and *Cxcr5*$^+$ LTiP (clusters 10, 11, and 12 at E13.5 and cluster 7 at E14.5) (Figure S5), with most cells being αLPs rather than LTiPs within the FL. Very few cells were associated with LTi$_0$ or LTi$_4$ stages at E13.5 (*Ccr6*$^+$ cells in cluster 11 at E13.5 and cluster 4 at E14.5). At E13.5, analysis of differentiation using velocity (La Manno et al., 2018) revealed flow from αLPs toward LTiPs (from cluster3 toward clusters 10 and 12; Figure S5C). At E14.5, however, velocity directions were not strong from αLPs toward LTi cells (within *aLP* cluster 2 toward cluster 7; Figure S5G). Moreover, LTi cluster 4 at E14.5 was completely separated from the other LTi$_4$ population. Within the periphery, at E13.5, we observed *Flt3*$^+$*Id2*$^-$ CLP and *Itga4*$^+$*Id2*$^+$ αLP populations (clusters 6 and 10 and partially in cluster 2; Figures 4A and 4B) and substantially more LTiP cells. The LTiP population showed expression of proliferation genes, whereas LTi$_0$ and LTi$_4$ expressed genes associated with LTi stages, such as *Il22*, *Lta*, and *Cd4* (Figures 4B and S6). Proliferation is a strong nominator for clustering cells, showing about

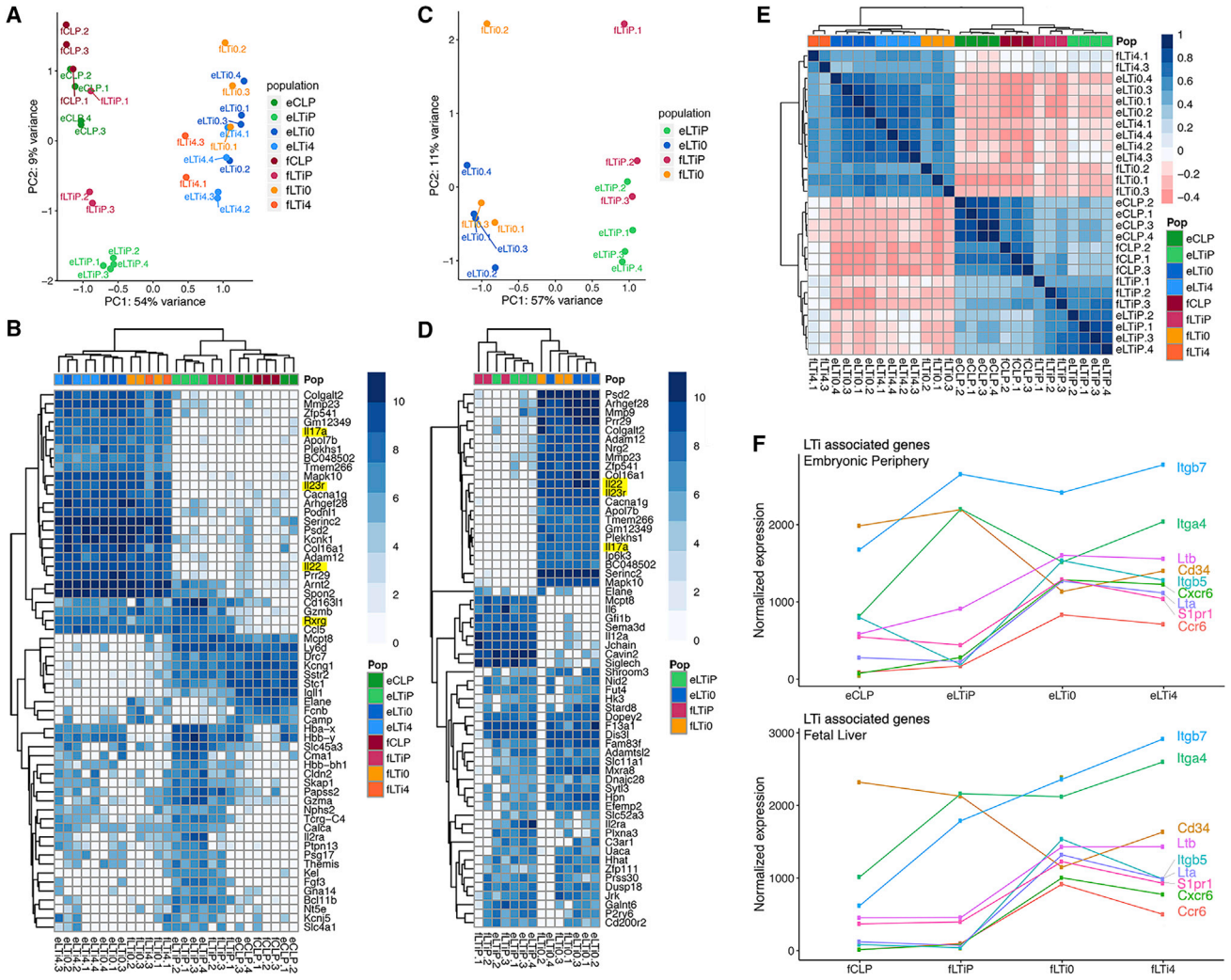

Figure 3. Gene Expression Profiling of the Populations in LTi Ontogeny in FL versus Embryonic Periphery

Populations in LTi ontogeny were sort-purified from the FL (f) and periphery (e) of E13.5 *RORγt*^{eGFP} embryos as f/e CLPs (Lin$^-$CD45$^+$IL7Rα$^+$α$_4$β$_7^+$RORγt$^-$CD4$^-$), f/e LTiPs (Lin$^-$CD45$^+$IL7Rα$^+$α$_4$β$_7^+$RORγt$^+$CD4$^-$), f/e LTi$_0$ (Lin$^-$CD45$^+$IL7Rα$^+$α$_4$β$_7^+$RORγt$^+$CD4$^-$), and f/e LTi$_4$ (Lin$^-$CD45$^+$IL7Rα$^+$α$_4$β$_7^+$RORγt$^+$CD4$^+$). For the gating strategies, see Figure S3A for FL and Figure S3B for embryonic periphery, enriched for peripheral LN anlagen.

(A) PCA of all populations from the FL and embryonic periphery. The largest variation is observed between CLPs and LTiPs versus LTi$_0$ and LTi$_4$, with 54% of the total variance explained by PC1.

(B) Heatmap of gene expression of all LTi populations using the 30 best loading genes of the two first principal components of the PCA and hierarchical clustering on rows and columns. We observed clustering based on stage in ontogeny rather than tissue of origin.

(C) PCA of LTiP and LTi$_0$ populations from the FL and embryonic periphery. The largest variation is observed between LTiPs versus LTi$_0$ independent of the tissue, with 57% of the total variance explained by PC1.

(D) Heatmap of gene expression of all LTiP and LTi$_0$ populations using the 30 best loading genes of the two first principal components of the PCA and hierarchical clustering on rows and columns.

(E) Correlation matrix to quantify the differences or similarities between the populations and origin tissue based on the 30 best loading genes of each population.

(F) Evolutionary gene pattern expression plots of the separate populations based on the bulk sequencing data, with specific gene expression in the different stages of LTi ontogeny in the periphery showing LTi-associated genes in the embryonic periphery or FL. See also Figures S3C–S3F.

Data shown are based on at least 2 independent flow cytometry sorts and experiments. FL fCLP, fLTiP, and fLTi0, n = 3; fLTi4, n = 2; embryonic peripheral cells (eCLP, eLTiP, eLTi$_0$, and eLTi$_4$), n = 4.

half of the *Flt3*$^+$*Id2*$^-$ CLPs in proliferation (cluster 10) and the LTiP population (cluster 4), supporting the proliferation assay results (Figure 2D). Cluster 2 was a mix of non-proliferative αLP and LTiP cells, based on partial expression of *Cxcr6* and *Cxcr5* (Figures 4B and S6). Using velocity, we observed a differentiation from CLP-αLP toward LTiP cells (cluster 2). Cluster 8 could be a different source for ILC-precursor (ILCp) and LTiP cells, being a separate source of progenitors other than cluster 6 (Figures 4A and 4C), and this cluster was connected to proliferative LTiP cluster 4. Besides the regular LTi-associated genes (Figures

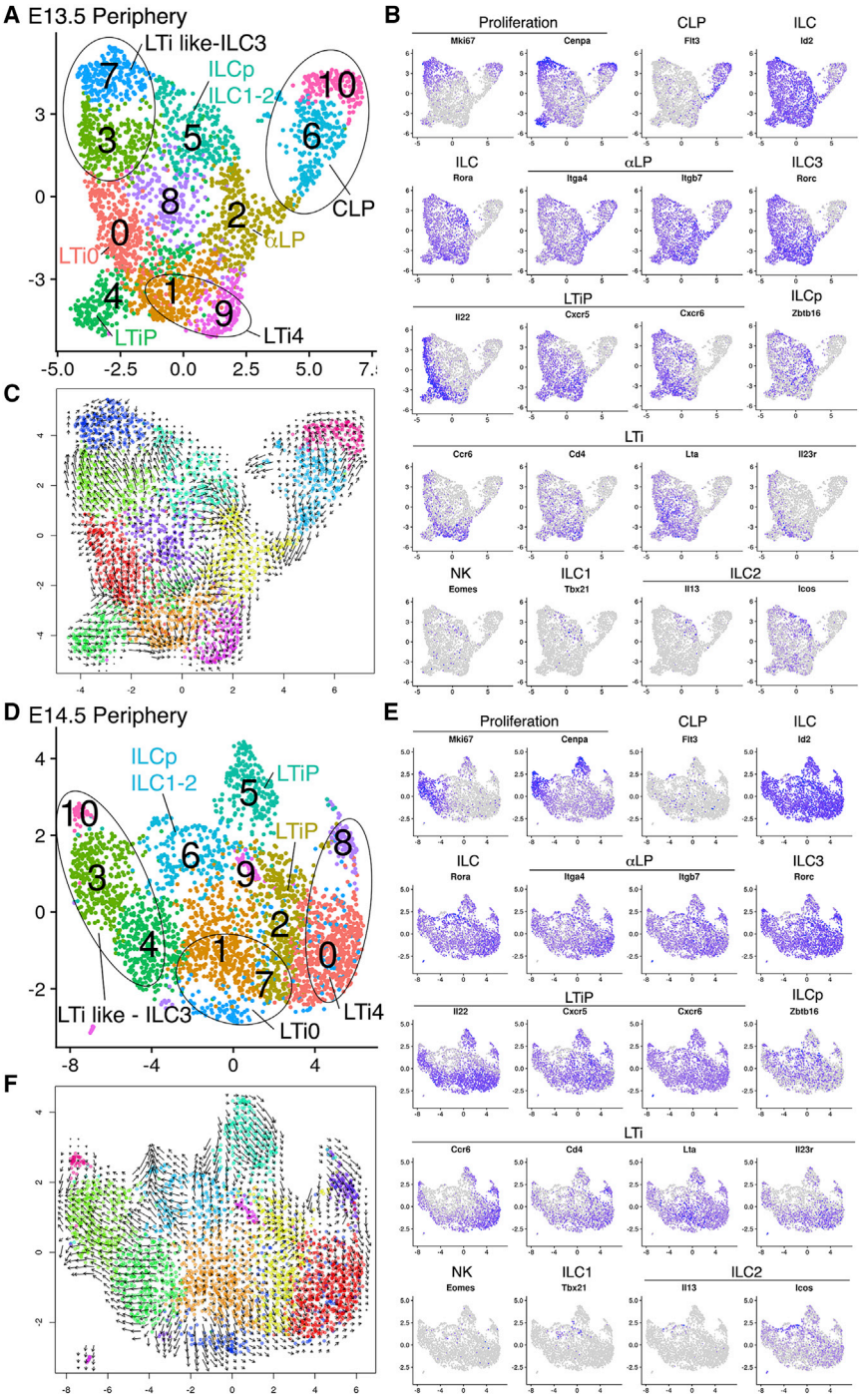

Figure 4. Single-Cell Sequencing of the Il7Rα$^+$ Population at E13.5 and E14.5

(A–F) Alive CD45$^+$F4/80$^-$Il7Rα$^+$ cells from E13.5 and E14.5 C57BL/6J embryo peripheries were sort-purified by flow cytometry, and a library of single-cell expression was generated using the 10x Genomics dropseq protocol. For the gating strategy, see Figures S4A and S4B for the periphery and Figures S4C and S4D for the FL. For single-cell results on FL, see Figures S5A–S5D for the E13.5 stage and Figures S5E–S5H for the E14.5 stage. E13.5 peripheral cells are shown in (A)–(C), whereas E14.5 is shown in (D)–(F).

(A and D) UMAP plot showing the cell clusters.

(B and E) Gene expression UMAP plots for population-annotated genes, listed per population. Violin plots of these genes, showing more detail regarding expression level and number of positive cells per cluster, are shown in Figure S6A for E13.5 and in Figure S7A for E14.5. The 10 most changed genes are shown in a heatmap in Figure S6B and in Figure S7B for E14.5.

(C and F) RNA velocity analysis (La Manno et al., 2018) based on the ratio of high nuclear RNA and processed RNA, allowing analysis of the direction of cell differentiation and aiding with determination of the populations.

4B, S6A, and S6B) in cluster 9, we also saw higher expression of major histocompatibility complex MHC) class II-associated genes, such as *H2-Ab1* (see the heatmap in Figure S6B). On the contrary, *H2-Ab1* expression was less pronounced in LTi$_4$ cluster 1. At E14.5, the most notable difference was the lack of CLPs within the periphery but still observed in the FL. It is likely that Il7Rα$^+\alpha_4\beta_7^-$ cells observed in flow cytometry (Figure 2B) mostly represent non-ILC commmitted CLPs. Also, an *Itga4*$^+$*Id2*$^+$*Cxcr6*$^-$ αLP cluster was not observed, based on gene expression (Figures 4D, 4E, S7A and S7B) and velocity analysis (Figure 4F). We observed a LTiP population (proliferating cluster 5, non-proliferative in cluster 2) and 2 LTi$_0$ and LTi$_4$ clusters. Besides lacking ILC-committed CLPs and αLP, E14.5 clusters resembled E13.5 but revealed more and more distant LTi populations within the Uniform Manifold Approximation and Projection (UMAP) plot, such as the LTi$_4$ population highly expressing *H2-Ab1* and *H2-Eb1* (cluster 8; Figures 4D, S6B, and 7C). At E13.5 and E14.5, we did not observe a natural killer (NK)-dedicated (*Eomes*$^+$) or ILC1-dedicated (*Tbx21*$^+$ [Tbet]) cluster and few ILCp (*Zbtb16*$^+$) or ILC2 (*Il13*$^+$*Icos*$^+$) cells. All of these cells were grouped together in cluster 5 at E13.5 or cluster 6 at E14.5. ILC3 or LTi-like cells were identified separately from LTi cells, based on much lower *Il23r*, *Ccr6*, *Cd4*, and *LTa* expression levels and fewer positive cells within the clusters (3 and 7 at E13.5 and 3, 4, and 10 at E14.5) (Figures 4A, S6A, and S7A). In general, we identified most CLP and αLP cells within the FL and most LTi cells within the periphery, confirming earlier flow cytometry results. There is some ambiguity regarding the connection of the LTiP, ILCp, and ILC3 clusters, possibly because of the previous described dynamic nature of ILC differentiation (Ishizuka et al., 2016b; Walker et al., 2019). The main populations within

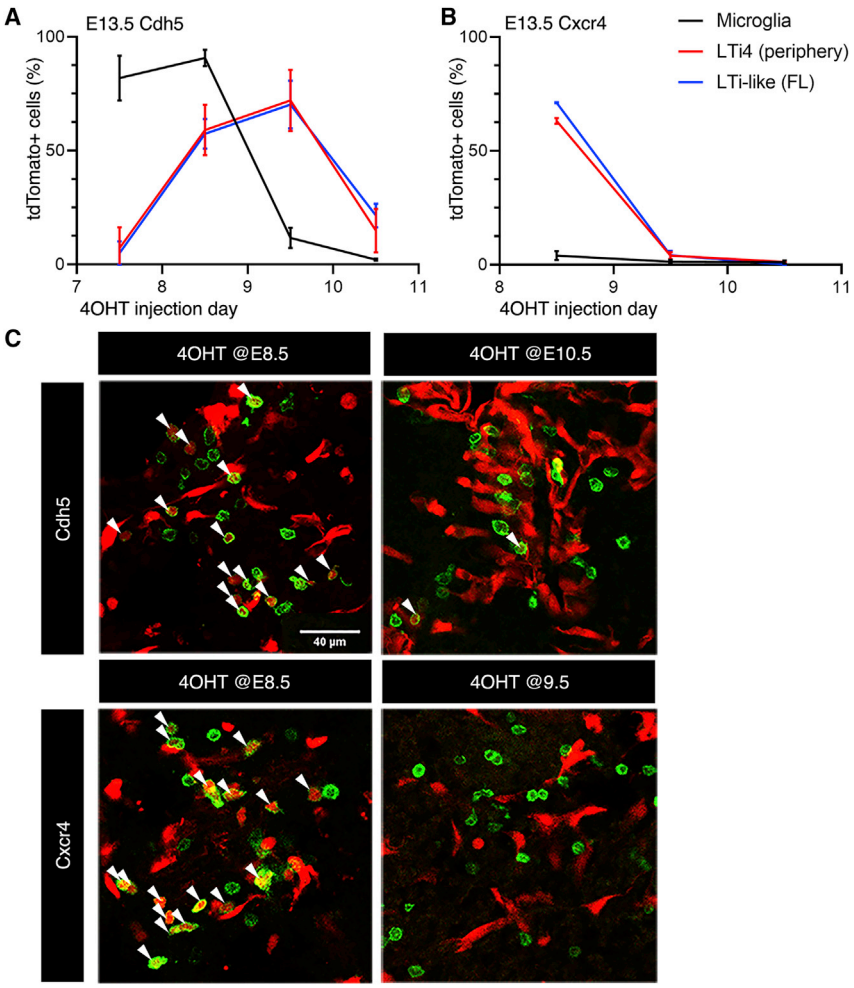

Figure 5. Hematopoietic Origin of LTi Cells during Embryonic LN Formation

(A and B) Recombination within LTi_4 cells ($CD45^+F4/80^-IL7R\alpha^+\alpha_4\beta_7^+CD4^+$) in the periphery and LTi-like cells ($CD45^+F4/80^-IL7R\alpha^+\alpha_4\beta_7^+$) in the FL from E13.5 (A) *iCdh5*^{tdT} pulsed with 4OHT between E7.5 and E10.5 and (B) *iCxcr4*^{tdT} embryos pulsed with 4OHT between E8.5 and E10.5, measured by flow cytometry. See the flow cytometry strategies in Figures S8A–S8C.

(C) Immunofluorescence of fluorescent reporter (tdT) recombination and $CD4^+$ cells (green) in CLNs or MdLNs from E13.5 *iCdh5*^{tdT} embryos pulsed with 4OHT at E8.5 or E10.5 and *iCxcr4*^{tdT} embryos pulsed at E8.5 or E9.5. Arrows represent recombined $CD4^+$ cells.

Scale bars, 40 µm. Data shown are from at least two independent experiments and are shown as average ± SD. See also Figure S8D.

this analysis are LTi cells rather than ILC1s or ILC2s, indicating that, at this embryonic stage, αLPs in the FL and LTiPs in the periphery preferentially differentiate into LTi cells.

LTi Progenitors Are Generated from an Embryonic Hemogenic Endothelial Site

Hematopoietic progenitors appear at specific time points from the hemogenic endothelium in YS embryonic or hemogenic endothelial sites, such as the AGM region. We first used *Cdh5-CreERT2*$^{+/-}$*;Rosa*^{tdT} (Gentek et al., 2018; Zovein et al., 2008) (hereafter referred to as *iCdh5*^{tdT}) as a lineage tracing model. In this model, (hemogenic) endothelial cells from embryonic hemogenic sites or the YS and their respective hematopoietic progeny undergo recombination to express tdTomato depending on when 4-hydroxytamoxifen (4OHT) was injected. In general, YS hemogenic endothelium is labeled when 4OHT is injected between E7.5 and E9, whereas the embryonic hemogenic endothelium is labeled when injected between E8.5 and E11.5 (Gentek et al., 2018; Yoder, 2014). We analyzed recombination in embryos at E13.5, when LN anlagen formation had initiated and before the dramatic expansion of the LN cluster because of lymphotoxin signaling (Figures 1B and 1C). In the *iCdh5*^{tdT} model, 4OHT pulsing at E7.5 targets early YS hematopoiesis, resulting in efficient labeling of microglia (Gentek et al., 2018; Hoeffel et al., 2015; Zovein et al., 2008; Figure 5A). When pulsed at E8.5, microglia progenitors from the YS were still labeled. Also, at this stage, LTi_4 cells in the periphery and LTi-like cells within the FL were labeled. When 4OHT was injected at E9.5, microglia were hardly labeled at all, indicating that YS contribution occurred until E8.5. LTi_4 and LTi-like cells were still labeled very efficiently at this stage, whereas 4OHT injections at E10.5 hardly labeled LTi or LTi-like cells at all. These results would be in line with embryonic LTi being generated from late YS, early embryonic hematopoiesis, or a combination thereof. To discriminate between YS or embryonic hemogenic endothelial contributions, we used *Cxcr4-CreERT2*$^{+/-}$*;Rosa*^{tdT} (Werner et al., 2020) (hereafter referred to as *iCxcr4*^{tdT}). Because the YS endothelium does not express *Cxcr4*, this model labels embryonic hemogenic endothelium-derived cells when pulsed after E8 (McGrath et al., 1999; Park et al., 2018; Werner et al., 2020). To confirm that *Cxcr4* does not label YS-derived cells after E8, we pulsed *iCxcr4*^{tdT} at E8.5 and analyzed the embryo proper and YS at E9.5. We observed that, within the YS, no cells expressed tdT, whereas, within the embryo proper, 20% ± 9.8% of the total cell population was recombined (Figure S8D). In line with this, 4OHT administration between E8 and E9 induced only residual microglia labeling (Figure 5B), whereas we observed about 63% recombination within the LTi population using the same approach (Figure 5B). To confirm recombination of LTi cells *in situ* within the LN anlagen, we analyzed sections from *iCdh5*^{tdT} and *iCxcr4*^{tdT} embryos obtained from dams injected with 4OHT between E8.5 and E10.5. Indeed, the presence of $tdTomato^+CD4^+$ LTi_4 cells within the LN anlagen followed the results obtained by flow cytometry (Figure 5C). Collectively, the fate mapping data from the *iCdh5*^{tdT} or *iCxcr4*^{tdT} models

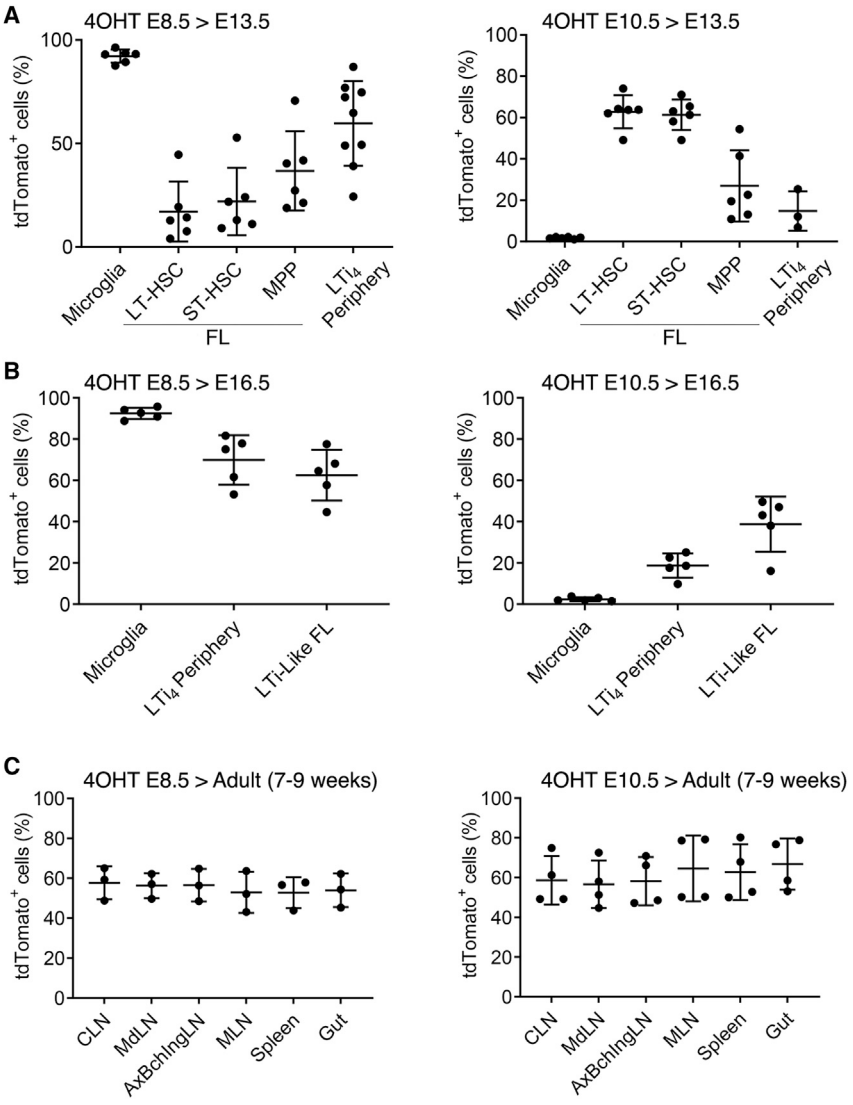

Figure 6. Embryonic LTi Cells Are Separate from the HSC Wave but Replaced by HSCs in Adults

(A) Recombination within microglia from the brain ($CD45^+F4/80^+$), long-term HSCs (LT-HSCs; defined as $Lin^-F4/80^-CD45^+CD11b^-c\text{-}Kit^+Sca\text{-}1^+CD48^-CD150^+$), short-term HSCs (ST-HSCs; defined as $Lin^-F4/80^-CD45^+CD11b^-c\text{-}Kit^+Sca\text{-}1^+CD48^-CD150^-$), and multipotent progenitors (MPPs; defined as $Lin^-F4/80^-CD45^+CD11b^-c\text{-}Kit^+Sca\text{-}1^-CD48^+CD150^-$) from the FL and LTi_4 cells from the periphery from E13.5 *iCdh5*^{tdT} embryos pulsed at E8.5 or E10.5, measured by flow cytometry.

(B) Microglia from the brain, LTi_4 cells ($CD45^+F4/80^-IL7R\alpha^+\alpha_4\beta_7^+CD4^+$) from the periphery, and LTi-like cells ($CD45^+F4/80^-IL7R\alpha^+\alpha_4\beta_7^+$) from the FL from E16.5 *iCdh5*^{tdT} embryos pulsed at E8.5 or E10.5, measured by flow cytometry.

(A and B) Data shown are from at least two independent experiments and are shown as average ± SD. Single data points represent individual embryos. See the flow cytometry strategies in Figures S8A–S8C and S8E.

(C) Recombination of tdTomato in LTi_4 cells ($Lin^-CD45^+IL7R\alpha^+CD4^+$) from various adult *iCdh5*^{tdT} lymphoid organs and gut, pulsed with 4OHT at E8.5 and E10.5 and measured by flow cytometry. LN AxBchIng is a pool of cells from the AxLNs, BrLNs, and inguinal peripheral LNs. See the flow cytometry strategies in Figures S9A–S9D.

See also Figures S9E and S9F. Each point represents an individual mouse. Data shown are from at least 3 mice and shown as average ± SD.

revealed that embryonic LTi cells are derived from early embryonic hematopoietic activity, most likely from the AGM region, but not from YS hematopoiesis.

Layered Production of LTi Progenitors

Progenitors for, e.g., macrophages (Hoeffel et al., 2015), ILC2s (Schneider et al., 2019), and mast cells (Gentek et al., 2018) differentiated from distinct and developmentally restricted HSCs. Therefore, we assessed whether LTi progenitor production was distinct from that of adult-type definitive HSCs; i.e., those that colonize the bone marrow, where they ultimately give rise to adult definitive hematopoietic lineages (Yoder, 2014). We compared the fate mapping kinetics of LTi progenitors and FL HSCs in E13.5 embryos that had been pulsed at E8.5 (the peak of LTi progenitor labeling) and at E10.5 (the peak of HSC labeling; Yoder, 2014) using the *iCdh5*^{tdT} model. When 4OHT was injected at E8.5, we observed high LTi_4 recombination, whereas the myeloid progenitor population (MPP) and long-term and short-term HSCs were recombined at lower rates (Figure 6A). Conversely, 4OHT injection at E10.5 resulted in very low LTi recombination, whereas recombination in both HSC populations was high (around 63%) (Figures 5A and 6A). Recombination in MPPs was between HSC and LTi_4 cells, indicating that they were probably appearing before the HSC but after the LTi population (Figure 6A). We conclude that embryonic LTi progenitors are produced prior to adult-type definitive HSCs.

It has been shown that, for ILC2s, different progenitors were responsible for the different waves of ILC2 development during late embryo gestation, neonatal life, and adulthood (Schneider et al., 2019). A dramatic increase in LN anlagen size occurs after E14.5, when the lymphotoxin pathway has been activated (van de Pavert and Mebius, 2010). We reasoned that LTi cells involved during initiation might be different and, thus, from a different hematopoietic wave than those during expansion and establishment of the LN anlagen. We analyzed LTi recombination in *iCdh5*^{tdT} embryos at late gestation (E16.5), pulsed at E8.5 or E10.5 (Figure 6B). The recombination rates followed those obtained when analyzed at E13.5. However, compared with peripheral LTi cells, we noted a slight increase in recombination of $CD45^+F4/80^-Il7R\alpha^+\alpha_4\beta_7^+$ LTi-like cells in the FL when injected

at E10.5 (Figure 6B), possibly attributable to non-LTi ILC progenitors present within this population at this stage. We conclude that all progenitors for embryonic LTi cells were efficiently labeled in the embryonic hemogenic endothelium around E8.5 in the *iCdh5*^{tdT} model.

LTi cells have a half-life of 22–26 days (Sawa et al., 2010) and, thus, need to be replaced during life, similarly as shown previously for ILC2s or mast cells (Gentek et al., 2018; Schneider et al., 2019). To establish whether LTi cells derived from the E8.5 embryonic wave are replaced in the adult by cells derived from HSCs, we analyzed recombination in LTi$_4$ cells within adult *iCdh5*^{tdT} lymphoid organs and gut when the mothers of these mice were injected with 4OHT at E8.5 and E10.5. In these adult mice, microglia behaved similarly as in the embryonic stages analyzed (Figures 5A, 6C, and S9E). Definitive hematopoietic lineages in adult blood were found to be recombined at lower rates when 4OHT was injected at E8.5 compared with E10.5, as shown before (Gentek et al., 2018; Figure S9E). The HSCs in the bone marrow followed the recombination rates observed for definitive lineages (Figure S9F). For analysis of recombination in LTi$_4$ cells, we used several lymphoid organs. When 4OHT was injected at E8.5, we observed that recombination was around 60% in all LTi$_4$ cells (Figure 6C), similar as for LTi cell recombination at embryonic time points analyzed (Figures 5A and 6A). When 4OHT was injected at E10.5, we also observed around 60% recombination in LTi$_4$ cells in all lymphoid organs studied, which is similar to definitive lineages and HSCs at this injection time point (Figure S9F) and much higher than when analyzed at E10.5 (Figure 6B). In summary, we observed high recombination in LTi cells in embryos at E13.5 and E16.5 when 4OHT was injected only at E8.5 but not when injected at E10.5 (Figures 6A and 6B). Conversely, using the same approach, analysis of LTi cells in adult lymphoid organs revealed that, when 4OHT was injected at E10.5, high recombination was observed in these LTi cells as well. Because the HSCs and definitive lineages were also labeled at a similar percentage, these data suggest that Lti cells in the adult are replaced by HSC-derived cells.

Collectively, *iCdh5*^{tdT} and *iCxcr4*^{tdT} fate mapping established that embryonic LTi cells originate from early hematopoietic activity in embryonic hemogenic endothelial sites, independent of the YS and independent of adult-type definitive hematopoiesis. Similar to other innate immune lineages, such as macrophages and mast cells (Gentek et al., 2018; Hoeffel et al., 2015), in the adult, LTi cells are replaced by cells from definitive HSCs.

DISCUSSION

LTi cells are the first cells of the ILC family to appear during embryogenesis and are essential for LN organogenesis. Nonetheless, their precise ontogeny is not known. In this study, we identified the kinetics of differentiation and the respective embryonic locations.

Using 3D imaging of the complete embryo, we showed that LTi$_0$ and LTi$_4$ cells aggregate at specific niches within the embryo. This method allows better quantification compared with flow cytometry because only cells within the cluster are counted and not single cells situated outside of the LN anlagen, providing accurate quantification of LTi cells associated with LN anlagen. Clustering occurred in a time-wise and anterior-to-posterior patterning that followed the chronicity as was studied by blocking lymphotoxin signaling (Rennert et al., 1998). However, our method is a refinement and enables much more comprehensive identification of LN anlagen formation, well before lymphotoxin signaling.

In LTi ontogeny, the known stages before LTi$_0$ are the αLP or LTiP stage and CLP stage (Ishizuka et al., 2016b, 2016a). To establish the presence of the CLP and LTiP populations and assess linear progress in LTi cell differentiation between FL versus periphery, we thoroughly examined these populations in both organs by flow cytometry and transcriptional profiling. We first observed CLP and a few LTiP cells within the FL at E11.5 but no LTi$_0$ nor LTi$_4$ cells. CLPs were predominantly present within the FL, whereas LTiP cells were equally present in the FL and periphery. Based on these numbers and CLP plus LTiP proliferation rates being especially high within the FL, we conclude that, starting at the CLP stage and especially at LTiP stages, the cells migrate out of the FL to the periphery, where they are exposed to retinoic acid to induce RORγt (van de Pavert et al., 2014). The transcriptional profile of the LTi$_0$ stage, in which *Rorc* is expressed, was associated with expression of retention and transcription factors and thus established LTi cell identity within the periphery. At later embryonic stages, most LTi$_0$ and LTi$_4$ cells were present within the periphery, and hardly any were observed within the FL, as confirmed by single-cell sequencing. Transcriptional profiling revealed that the LTi$_0$ and LTi$_4$ populations in the FL and periphery were remarkably similar; thus, based on these data, we propose that LTi$_0$ or LTi$_4$ cells within the periphery are most likely not a progression in ontogeny from the FL.

To obtain more insights in LTi cell ontogeny, we performed RNA velocity analysis of the ILC population within the FL and periphery. We were able to separate the αLP population from the LTiPs and determined a hierarchical link between αLPs being mostly found in FL and LTiPs mostly observed within the periphery. The LTi$_0$ and LTi$_4$ populations were mainly observed within the periphery. This process of tissue-specific differentiation within the embryo has been shown before for macrophages (Mass et al., 2016). Interestingly, we observed 2 different LTi$_4$ populations, not discriminable by fluorescence-activated cell sorting (FACS), based on MHC class II-associated genes for E13.5 and E14.5. It has been shown that ILC3-like or LTi-like cells present MHC class II and have antigen-presenting capabilities, especially within the gut (Hepworth et al., 2013; Mackley et al., 2015), and we observed a divergence already present at E13.5. Future studies should reveal a difference in their LN-forming versus possible antigen-presenting capacities.

The αLP population was highly dynamic and mainly gave rise to LTiPs, LTi cells, and, to a lesser extent, ILC2, ILCp, and ILC3 cells but not ILC1 cells at this embryonic stage. It is possible that the same progenitors are able to divert into other ILCs at other developmental stages when provided with the proper external stimuli, as also shown before (Ishizuka et al., 2016b; Koga et al., 2018).

Using an established *Cdh5-CreERT2* and a *Cxcr4-CreERT2* mouse lineage tracing model (Werner et al., 2020), we showed

that the majority of embryonic LTi progenitors appeared from an embryonic hemogenic endothelial site but not from the YS hemogenic endothelium. The AGM region is the most-studied and best-defined embryonic hemogenic endothelial site. Hemogenic endothelial sites have been observed outside of the AGM region, like the head and heart, but most of the hematopoietic clusters in these areas appeared later than the LTi progenitors at E8.5 (Shigeta et al., 2019; Yzaguirre and Speck, 2016). Notably, the vitelline artery, connected to the dorsal aorta in the AGM, showed hematopoietic clusters (Yokomizo et al., 2011; Yzaguirre and Speck, 2016; Zovein et al., 2010). Therefore, we cannot exclude other embryonic hemogenic sites from which LTi progenitors could appear.

We confirmed that, at E9.5, the *iCxcr4*^{tdT} model shows a transient lower recombination efficiency (Werner et al., 2020) compared with the *iCdh5*^{tdT} model. *Cxcr4* expression has been shown to fluctuate within early hematopoiesis (Baron et al., 2018), and, therefore, the lower efficiency in this model at E9.5 could be due to transient lower *Cxcr4* expression in the embryonic hemogenic endothelium. Based on recombination in HSCs using the *iCdh5*^{tdT} model, which started after E10.5 and after appearance of LTi progenitors, we conclude that the LTi progenitor wave is separated from the HSC wave, making LTi progenitors one of the first lineages to appear from the embryonic hemogenic endothelium. During adulthood, LTi cells within lymphoid organs had similar recombination rates as the definitive lineages and HSCs. Therefore, we conclude that embryonic LTi cells are replaced in adulthood by HSC-derived cells. It has been shown that embryonic LTi and ILC3 cells have a half-life of around 24 days (Sawa et al., 2010); thus, they are likely to be replaced starting around 2 weeks after birth, at a time when the definitive hematopoietic lineages are starting to appear from the bone marrow (Gao et al., 2018). Other members of the ILC family have been shown to be derived from bone marrow HSCs; however, LTi cells derived from bone marrow HSCs were not observed before (Sawa et al., 2010; Schneider et al., 2019; Walker et al., 2019; Xu et al., 2019). The functional difference between embryonic and adult LTi cells is not known. Tertiary lymphoid formation does not require LTi cells (Drayton et al., 2006), but a specific role of LTi cells has been described in regeneration of the spleen after inflammation (Scandella et al., 2008). Thus, the main function of the embryonic LTi cells is to organize embryonic LN formation, whereas, in the adult, the role of LTi cells is unclear.

In this study, we were able to pinpoint the release of the earliest hematopoietic progenitor for an ILC-related lineage from the embryonic hemogenic endothelium, most likely the AGM region but not from the YS hemogenic endothelium and separated from the definitive HSC wave. The model we used will be of interest to other studies in which the specific contribution of embryonic hemogenic endothelial sites needs to be analyzed to understand the highly organized release of hematopoietic progenitors in time and location. For the LTi ontogeny, we propose that their hematopoietic progenitors arrive in the FL after E8.5 and differentiate toward the CLP stage. The subsequent αLP/LTiP cells migrate from the FL, and αLPs preferentially differentiate into LTi cells at E13.5, but to a much lesser extend than other ILC members at this embryonic stage. The FL could already provide cues to skew progenitors toward a more LTi phenotype, which is established by RORγt expression induced within the periphery. It will be essential to understand which processes occur in space and time and especially within the FL to guide cell fate into LTi or other ILC lineages at later embryonic stages and whether these embryonic ILCs will be replaced by HSC-derived cells.

STAR★METHODS

Detailed methods are provided in the online version of this paper and include the following:

- KEY RESOURCES TABLE
- RESOURCE AVAILABILITY
  - Lead Contact
  - Materials Availability
  - Data and Code Availability
- EXPERIMENTAL MODEL AND SUBJECT DETAILS
  - Mice
- METHOD DETAILS
  - Timed pregnancies and Tamoxifen administration
  - Flow-cytometry
  - Immunofluorescence
  - Whole mount preparation and analysis
  - EdU proliferation assay
  - Next generation sequencing
- QUANTIFICATION AND STATISTICAL ANALYSIS
  - Quantification of LN formation
  - Statistical analysis

SUPPLEMENTAL INFORMATION

Supplemental Information can be found online at https://doi.org/10.1016/j.celrep.2020.108004.

ACKNOWLEDGMENTS

This work was supported by FRM Amorçage de jeunes équipes (AJE20150633331), ANR ACHN (ANR-16-ACHN-0011), ANR PRCI (ANR-17-CE13-0029-01), and A*midex Chaire d'excellence (to S.A.v.d.P.) and institutional grants from INSERM, CNRS, and Aix-Marseille University (to the CIML). We acknowledge the PICSL imaging facility of the CIML (ImagImm), a member of the national infrastructure France-BioImaging supported by the French National Research Agency (ANR-10-INBS-04), notably Mathieu Fallet and Sebastian Mailfert. We thank Catherine Robin for fruitful discussions; Pierre Milpied, Laurine Gil, and the genomic core platform for help with single-cell sequencing; LABO'M for social support; the animal facility, notably Toufik Guelmami and Michel Pontier; the flow cytometry core facility, notably Atika Zouine, Sylvain Bigot, and Marc Barad; Lionel Chasson of the histology platform; Ralf Adams for use of *Cdh5-CreERT2*; Gérard Eberl for the kind donation of the *RORγt*^{eGFP} mice; Shinichi Nishikawa for the IL7Rα antibody clone; and Reina Mebius for past input.

AUTHOR CONTRIBUTIONS

M.S. performed the experiments, analyzed data, and wrote the manuscript. I.M., S.W., R.R.S., C.S., R. Gentek, M.G.-M., Y.M.K., L.d.F., and J.V. performed the experiments and analyzed data. L.S. analyzed sequencing data. Y.M.K., M.B., R.S., and R. Golub. provided key expertise and reagents.

S.A.v.d.P. performed experiments, analyzed data, wrote the manuscript, and supervised the project.

DECLARATION OF INTERESTS

The authors declare no competing interests.

Received: November 21, 2019
Revised: May 18, 2020
Accepted: July 16, 2020
Published: August 11, 2020

REFERENCES

Baron, C.S., Kester, L., Klaus, A., Boisset, J.-C., Thambyrajah, R., Yvernogeau, L., Kouskoff, V., Lacaud, G., van Oudenaarden, A., and Robin, C. (2018). Single-cell transcriptomics reveal the dynamic of haematopoietic stem cell production in the aorta. Nat. Commun. *9*, 2517.

Boisset, J.-C., van Cappellen, W., Andrieu-Soler, C., Galjart, N., Dzierzak, E., and Robin, C. (2010). In vivo imaging of haematopoietic cells emerging from the mouse aortic endothelium. Nature *464*, 116–120.

Chea, S., Schmutz, S., Berthault, C., Perchet, T., Petit, M., Burlen-Defranoux, O., Goldrath, A.W., Rodewald, H.-R., Cumano, A., and Golub, R. (2016). Single-Cell Gene Expression Analyses Reveal Heterogeneous Responsiveness of Fetal Innate Lymphoid Progenitors to Notch Signaling. Cell Rep. *14*, 1500–1516.

Drayton, D.L., Liao, S., Mounzer, R.H., and Ruddle, N.H. (2006). Lymphoid organ development: from ontogeny to neogenesis. Nat. Immunol. *7*, 344–353.

Gao, X., Xu, C., Asada, N., and Frenette, P.S. (2018). The hematopoietic stem cell niche: from embryo to adult. Development *145*, dev139691.

Gentek, R., Ghigo, C., Hoeffel, G., Bulle, M.J., Msallam, R., Gautier, G., Launay, P., Chen, J., Ginhoux, F., and Bajénoff, M. (2018). Hemogenic Endothelial Fate Mapping Reveals Dual Developmental Origin of Mast Cells. Immunity *48*, 1160–1171.e5.

Hepworth, M.R., Monticelli, L.A., Fung, T.C., Ziegler, C.G.K., Grunberg, S., Sinha, R., Mantegazza, A.R., Ma, H.-L., Crawford, A., Angelosanto, J.M., et al. (2013). Innate lymphoid cells regulate CD4+ T-cell responses to intestinal commensal bacteria. Nature *498*, 113–117.

Hoeffel, G., Chen, J., Lavin, Y., Low, D., Almeida, F.F., See, P., Beaudin, A.E., Lum, J., Low, I., Forsberg, E.C., et al. (2015). C-Myb(+) erythro-myeloid progenitor-derived fetal monocytes give rise to adult tissue-resident macrophages. Immunity *42*, 665–678.

Ishizuka, I.E., Constantinides, M.G., Gudjonson, H., and Bendelac, A. (2016a). The Innate Lymphoid Cell Precursor. Annu. Rev. Immunol. *34*, 299–316.

Ishizuka, I.E., Chea, S., Gudjonson, H., Constantinides, M.G., Dinner, A.R., Bendelac, A., and Golub, R. (2016b). Single-cell analysis defines the divergence between the innate lymphoid cell lineage and lymphoid tissue-inducer cell lineage. Nat. Immunol. *17*, 269–276.

Koga, S., Hozumi, K., Hirano, K.I., Yazawa, M., Terooatea, T., Minoda, A., Nagasawa, T., Koyasu, S., and Moro, K. (2018). Peripheral PDGFRα^{+}gp38^{+} mesenchymal cells support the differentiation of fetal liver-derived ILC2. J. Exp. Med. *215*, 1609–1626.

La Manno, G., Soldatov, R., Zeisel, A., Braun, E., Hochgerner, H., Petukhov, V., Lidschreiber, K., Kastriti, M.E., Lönnerberg, P., Furlan, A., et al. (2018). RNA velocity of single cells. Nature *560*, 494–498.

Lancrin, C., Sroczynska, P., Stephenson, C., Allen, T., Kouskoff, V., and Lacaud, G. (2009). The haemangioblast generates haematopoietic cells through a haemogenic endothelium stage. Nature *457*, 892–895.

Mackley, E.C., Houston, S., Marriott, C.L., Halford, E.E., Lucas, B., Cerovic, V., Filbey, K.J., Maizels, R.M., Hepworth, M.R., Sonnenberg, G.F., et al. (2015). CCR7-dependent trafficking of RORγ^{+} ILCs creates a unique microenvironment within mucosal draining lymph nodes. Nat. Commun. *6*, 5862.

Madisen, L., Zwingman, T.A., Sunkin, S.M., Oh, S.W., Zariwala, H.A., Gu, H., Ng, L.L., Palmiter, R.D., Hawrylycz, M.J., Jones, A.R., et al. (2010). A robust and high-throughput Cre reporting and characterization system for the whole mouse brain. Nat. Neurosci. *13*, 133–140.

Mass, E., Ballesteros, I., Farlik, M., Halbritter, F., Günther, P., Crozet, L., Jacome-Galarza, C.E., Händler, K., Klughammer, J., Kobayashi, Y., et al. (2016). Specification of tissue-resident macrophages during organogenesis. Science *353*, aaf4238.

McGrath, K.E., Koniski, A.D., Maltby, K.M., McGann, J.K., and Palis, J. (1999). Embryonic expression and function of the chemokine SDF-1 and its receptor, CXCR4. Dev. Biol. *213*, 442–456.

McGrath, K.E., Frame, J.M., and Palis, J. (2015a). Early hematopoiesis and macrophage development. Semin. Immunol. *27*, 379–387.

McGrath, K.E., Frame, J.M., Fegan, K.H., Bowen, J.R., Conway, S.J., Catherman, S.C., Kingsley, P.D., Koniski, A.D., and Palis, J. (2015b). Distinct Sources of Hematopoietic Progenitors Emerge before HSCs and Provide Functional Blood Cells in the Mammalian Embryo. Cell Rep. *11*, 1892–1904.

Park, M.A., Kumar, A., Jung, H.S., Uenishi, G., Moskvin, O.V., Thomson, J.A., and Slukvin, I.I. (2018). Activation of the Arterial Program Drives Development of Definitive Hemogenic Endothelium with Lymphoid Potential. Cell Rep. *23*, 2467–2481.

Rankin, L.C., Girard-Madoux, M.J.H., Seillet, C., Mielke, L.A., Kerdiles, Y., Fenis, A., Wieduwild, E., Putoczki, T., Mondot, S., Lantz, O., et al. (2016). Complementarity and redundancy of IL-22-producing innate lymphoid cells. Nat. Immunol. *17*, 179–186.

Rennert, P.D., James, D., Mackay, F., Browning, J.L., and Hochman, P.S. (1998). Lymph node genesis is induced by signaling through the lymphotoxin beta receptor. Immunity *9*, 71–79.

Sawa, S., Cherrier, M., Lochner, M., Satoh-Takayama, N., Fehling, H.J., Langa, F., Di Santo, J.P., and Eberl, G. (2010). Lineage relationship analysis of RORgammat+ innate lymphoid cells. Science *330*, 665–669.

Scandella, E., Bolinger, B., Lattmann, E., Miller, S., Favre, S., Littman, D.R., Finke, D., Luther, S.A., Junt, T., and Ludewig, B. (2008). Restoration of lymphoid organ integrity through the interaction of lymphoid tissue-inducer cells with stroma of the T cell zone. Nat. Immunol. *9*, 667–675.

Schneider, C., Lee, J., Koga, S., Ricardo-Gonzalez, R.R., Nussbaum, J.C., Smith, L.K., Villeda, S.A., Liang, H.-E., and Locksley, R.M. (2019). Tissue-Resident Group 2 Innate Lymphoid Cells Differentiate by Layered Ontogeny and In Situ Perinatal Priming. Immunity *50*, 1425–1438.e5.

Seillet, C., Mielke, L.A., Amann-Zalcenstein, D.B., Su, S., Gao, J., Almeida, F.F., Shi, W., Ritchie, M.E., Naik, S.H., Huntington, N.D., et al. (2016). Deciphering the Innate Lymphoid Cell Transcriptional Program. Cell Rep. *17*, 436–447.

Shigeta, A., Huang, V., Zuo, J., Zhou, B., Shigeta, A., Huang, V., Zuo, J., Besada, R., Nakashima, Y., Lu, Y., et al. (2019). Endocardially Derived Macrophages Are Essential for Valvular Remodeling Article Endocardially Derived Macrophages Are Essential for Valvular Remodeling. Dev. Cell *48*, 617–630.e3.

Sörensen, I., Adams, R.H., and Gossler, A. (2009). DLL1-mediated Notch activation regulates endothelial identity in mouse fetal arteries. Blood *113*, 5680–5688.

Sparwasser, T., Gong, S., Li, J.Y.H., and Eberl, G. (2004). General method for the modification of different BAC types and the rapid generation of BAC transgenic mice. Genesis *38*, 39–50.

van de Pavert, S.A., and Mebius, R.E. (2010). New insights into the development of lymphoid tissues. Nat. Rev. Immunol. *10*, 664–674.

van de Pavert, S.A., and Vivier, E. (2016). Differentiation and function of group 3 innate lymphoid cells, from embryo to adult. Int. Immunol. *28*, 35–42.

van de Pavert, S.A., Olivier, B.J., Goverse, G., Vondenhoff, M.F., Greuter, M., Beke, P., Kusser, K., Höpken, U.E., Lipp, M., Niederreither, K., et al. (2009). Chemokine CXCL13 is essential for lymph node initiation and is induced by retinoic acid and neuronal stimulation. Nat. Immunol. *10*, 1193–1199.

van de Pavert, S.A., Ferreira, M., Domingues, R.G., Ribeiro, H., Molenaar, R., Moreira-Santos, L., Almeida, F.F., Ibiza, S., Barbosa, I., Goverse, G., et al.

(2014). Maternal retinoids control type 3 innate lymphoid cells and set the offspring immunity. Nature *508*, 123–127.

Veiga-Fernandes, H., Coles, M.C., Foster, K.E., Patel, A., Williams, A., Natarajan, D., Barlow, A., Pachnis, V., and Kioussis, D. (2007). Tyrosine kinase receptor RET is a key regulator of Peyer's patch organogenesis. Nature *446*, 547–551.

Vivier, E., Artis, D., Colonna, M., Diefenbach, A., Di Santo, J.P., Eberl, G., Koyasu, S., Locksley, R.M., McKenzie, A.N.J., Mebius, R.E., et al. (2018). Innate Lymphoid Cells: 10 Years On. Cell *174*, 1054–1066.

Vondenhoff, M.F., Greuter, M., Goverse, G., Elewaut, D., Dewint, P., Ware, C.F., Hoorweg, K., Kraal, G., and Mebius, R.E. (2009). LTbetaR signaling induces cytokine expression and up-regulates lymphangiogenic factors in lymph node anlagen. J. Immunol. *182*, 5439–5445.

Walker, J.A., Clark, P.A., Crisp, A., Barlow, J.L., Szeto, A., Ferreira, A.C.F., Rana, B.M.J., Jolin, H.E., Rodriguez-Rodriguez, N., Sivasubramaniam, M., et al. (2019). Polychromic Reporter Mice Reveal Unappreciated Innate Lymphoid Cell Progenitor Heterogeneity and Elusive ILC3 Progenitors in Bone Marrow. Immunity *51*, 104–118.e7.

Werner, Y., Mass, E., Ashok Kumar, P., Ulas, T., Händler, K., Horne, A., Klee, K., Lupp, A., Schütz, D., Saaber, F., et al. (2020). Cxcr4 distinguishes HSC-derived monocytes from microglia and reveals monocyte immune responses to experimental stroke. Nat. Neurosci. *23*, 351–362.

Xu, W., Cherrier, D.E., Chea, S., Vosshenrich, C., Serafini, N., Petit, M., Liu, P., Golub, R., and Di Santo, J.P. (2019). An Id2^{RFP}-Reporter Mouse Redefines Innate Lymphoid Cell Precursor Potentials. Immunity *50*, 1054–1068.e3.

Yoder, M.C. (2014). Inducing definitive hematopoiesis in a dish. Nat. Biotechnol. *32*, 539–541.

Yokomizo, T., Ng, C.E.L., Osato, M., and Dzierzak, E. (2011). Three-dimensional imaging of whole midgestation murine embryos shows an intravascular localization for all hematopoietic clusters. Blood *117*, 6132–6134.

Yzaguirre, A.D., and Speck, N.A. (2016). Insights into blood cell formation from hemogenic endothelium in lesser-known anatomic sites. Dev. Dyn. *245*, 1011–1028.

Zovein, A.C., Hofmann, J.J., Lynch, M., French, W.J., Turlo, K.A., Yang, Y., Becker, M.S., Zanetta, L., Dejana, E., Gasson, J.C., et al. (2008). Fate tracing reveals the endothelial origin of hematopoietic stem cells. Cell Stem Cell *3*, 625–636.

Zovein, A.C., Turlo, K.A., Ponec, R.M., Lynch, M.R., Chen, K.C., Hofmann, J.J., Cox, T.C., Gasson, J.C., and Iruela-Arispe, M.L. (2010). Vascular remodeling of the vitelline artery initiates extravascular emergence of hematopoietic clusters. Blood *116*, 3435–3444.

STAR★METHODS

KEY RESOURCES TABLE

REAGENT or RESOURCE	SOURCE	IDENTIFIER
Antibodies		
Rat anti-mouse CD45 (clone 30-F11), BUV395	BD biosciences	Cat#564279; RRID:AB_2651134
Rat anti-mouse CD45 (clone 30-F11), PeCy7	Ebioscience	Cat#25-0451-82; RRID:AB_2734986
Rat anti-mouse F4/80 (clone T45-2342), BV510	BD biosciences	Cat#743280; RRID:AB_2741398
Rat anti-mouse F4/80 (clone BM8), BV785	Biolegend	Cat#BLE123141; RRID:AB_2563667
Rat anti-mouse F4/80 (clone T45-2342), PE-CF594	BD biosciences	Cat#565613; RRID:AB_2734770
Rat anti-mouse CD11b (clone M1/70), FITC	Ebioscience	Cat#11-0112-85; RRID:AB_464936
Rat anti-mouse CD11b (clone M1/70), V500	BD biosciences	Cat#562128; RRID:AB_10896991
Rat anti-mouse CD11b (clone M1/70), BV605	BD biosciences	Cat#563015; RRID:AB_2737951
Rat anti-mouse IL7Rα (clone A7R34), eFluor 660	Ebioscience	Cat#50-1271-80; RRID:AB_11218700
Rat anti-mouse CD4 (clone Gk1.5), PeCy7	Biolegend	Cat#BLE100422; RRID:AB_312707
Rat anti-mouse CD4 (clone Gk1.5), unlabeled	Ebioscience	Cat#14-0041-82; RRID:AB_467063
Rat anti-mouse α4β7 (clone DATK32), BV786	BD biosciences	Cat#740892; RRID:AB_2740540
Armenian hamster anti-mouse CD3e (clone 145-2C11), Alexa Fluor 488	Ebioscience	Cat#53-0031-82; RRID:AB_469889
Hamster anti-mouse CD3e (clone 145-2C11), BV510	BD biosciences	Cat#563024; RRID:AB_2737959
Hamster anti-mouse CD3e (clone 145-2C11), PE-CF594	BD biosciences	Cat#562286; RRID:AB_11153307
Rat anti-mouse CD19 (clone eBio1D3), FITC	Ebioscience	Cat#11-0193-82; RRID:AB_657666
Rat anti-mouse CD19 (clone 1D3), BV510	BD biosciences	Cat#562956; RRID:AB_2737915
Rat anti-mouse CD19 (clone 1D3), PE-CF594	BD biosciences	Cat#562291; RRID:AB_11154223
Rat anti-mouse CD8α (clone 53-6.7), V500	BD biosciences	Cat#560776; RRID:AB_1937317
Rat anti-mouse CD8α (clone 53-6.7), PE-CF594	BD biosciences	Cat#562283; RRID:AB_11152075
Rat anti-mouse B220 (clone RA3-6B2), Alexa Fluor 488	Ebioscience	Cat#53-0452-82; RRID:AB_469907
Rat anti-mouse TER-119 (clone TER-119), FITC	Ebioscience	Cat#11-5921-82; RRID:AB_465311
Rat anti-mouse Ly-6G/Ly-6C (clone RB6-8C5), FITC	Ebioscience	Cat#11-5931-82; RRID:AB_465314
Rat anti-mouse Ly-6G (clone 1A8), BV510	Biolegend	Cat#BLE127633; RRID:AB_2562937
Rat anti-mouse Ly-6G (clone 1A8), PE-CF594	BD biosciences	Cat#562700; RRID:AB_2737730
Armenian hamster anti-mouse TCR β (clone H57-597), BV510	BD biosciences	Cat#563221; RRID:AB_2738078
Rat anti-mouse CD115 (clone AFS98), PeCy7	Biolegend	Cat#BLE135524; RRID:AB_2566460
Rat anti-mouse CD117 ('c-Kit')(clone 2B8), BV605	BD biosciences	Cat#563146; RRID:AB_2738028
Hamster anti-mouse CD48 (clone HM48-1), BV711	BD biosciences	Cat#740687; RRID:AB_2740373
Rat anti-mouse CD150 (clone TC15-12F12.2), PeCy7	Biolegend	Cat#BLE115914; RRID:AB_439797
Rat anti-mouse Sca-1 (clone D7), APC	Ebioscience	Cat#17-5981-82; RRID:AB_469487
Rat anti-mouse CD31 (clone 390), PerCP-eFluor710	Ebioscience	Cat#46-0311-80; RRID:AB_1834430
Mouse anti-mouse Tubulin beta-3 (clone TUJ1), Alexa Fluor 488	Biolegend	Cat#BLE801203; RRID:AB_2564757
Chicken anti-GFP, unlabeled	AVES	Cat#GFP-1020; RRID:AB_10000240
Donkey anti-rat, Alexa Fluor 488	Thermo fisher	Cat#A-21208; RRID:AB_2535794
Donkey anti-chicken, Cy3	Jackson immunoresearch	Cat#703-166-155; RRID:AB_2340364
Donkey anti-rat, Alexa 647	Jackson immunoresearch	Cat#712-605-153; RRID:AB_2340694
Biological Samples		
Normal Mouse Serum	Jackson Immunoresearch	Cat#015-000-120; RRID:AB_2337194
Normal Donkey Serum	Jackson Immunoresearch	Cat#017-000-121; RRID:AB_2337258
Fetal Bovine Serum	Sigma-Aldrich	Cat#F7524-500mL

(*Continued on next page*)

Continued

REAGENT or RESOURCE	SOURCE	IDENTIFIER
Chemicals, Peptides, and Recombinant Proteins		
4-Hydroxytamoxifen	Sigma-Aldrich	Cat#T176-50mg
Progesterone	Sigma-Aldrich	Cat#P0130-25mg
Peanut oil	Sigma-Aldrich	Cat#P2144-250mL
Liberase TM	Roche	Cat#05401127001
DNase I	Roche	Cat#11284932001
Collagenase from *Clostridium histolyticum*	Sigma-Aldrich	Cat#C2139-100mg
Percoll	Sigma-Aldrich	Cat#GE17-0891-02
CD45 MicroBeads, mouse	Miltenyi	Cat#130052301
SYTOX Blue Dead Cell Stain	Invitrogen	Cat#S34857
Zombie UV Fixable Viability dye	Biolegend	Cat#BLE423108
eBioscience 1X RBC Lysis Buffer	Ebioscience	Cat# 00-4333-57
FACS buffer	Homemade	N/A
HEPES	GIBCO	Cat#15630-80
UltraPure EDTA	Invitrogen	Cat#15576-028
Buffer A	Homemade	N/A
Buffer B	Homemade	N/A
PBS	Homemade	N/A
Acetone	Carlo Erba chemicals	Cat#301505
Methanol	Carlo Erba chemicals	Cat#412383
Benzyl alcohol	Honeywell	Cat#108006
Benzyl benzoate	Acros organics	Cat#105862500
Mowiol 4-88	Calbiochem	Cat#475904
Sucrose	Sigma-Aldrich	Cat#S9378
16% Paraformaldehyde solution	Delta microscopies	Cat#D15710
BSA	ID bio	Cat#1000-70
Triton X-100	Sigma-Aldrich	Cat#T8787-250mL
PBS-MT	Homemade	N/A
BABB	Homemade	N/A
Critical Commercial Assays		
Click-iT Plus Edu Alexa Fluor 594 Flow Cytometry Assay Kit	Invitrogen	Cat#C10646
Adult Brain Dissociation kit, mouse and rat	Miltenyi	Cat#130-107-677
Chromium Single Cell 3′ Library and Gel Bead Kit v2, 4 rxns	10x Genomics	Cat#120267
Chromium i7 Multiplex Kit, 96 rxns	10x Genomics	Cat#120262
Chromium Single Cell 3′ GEM, Library & Gel Bead Kit v3, 4 rxns	10x Genomics	Cat#1000092
SMART-Seq v4 Ultra Low Input RNA Kit for Sequencing	Clontech	Cat#634888
Agilent RNA 6000 Pico Kit	Agilent	Cat#5067-1513
High Sensitivity DNA Analysis Kit	Agilent	Cat#5067-4626
Qubit dsDNA HS Assay Kit	ThermoFisher	Cat#Q32854
Single cell RNA purification kit	Norgen Biotek Corp.	Cat#51800
Deposited Data		
Raw data	This paper	GEO: GSE153771
Analyzed sequencing data	This paper	https://github.com/CIML-bioinformatic/SPlab_BecomingLTi
Experimental Models: Organisms/Strains		
Mouse: C57BL/6J (JAX mice strain)	Charles River	Stock#632
Mouse: RjOrl:SWISS (‘CD1’)	Janvier Labs	https://www.janvier-labs.com/en/fiche_produit/swiss_mouse/

(*Continued on next page*)

Continued

REAGENT or RESOURCE	SOURCE	IDENTIFIER
Mouse: RORγt^{eGFP}	Sparwasser et al., 2004	Gift from Gérard Eberl
Mouse: *Cdh5-CreERT2*$^{+/-}$	Sörensen et al., 2009	Gift from Ralf Adams
Mouse: *Cxcr4-CreER*$^{+/-}$	Werner et al., 2020	N/A
Mouse: *Rosa*$^{tdTomato/\ tdTomato}$	Madisen et al., 2010; The Jackson Laboratory	Stock# 007914
Software and Algorithms		
FlowJo version 10.5.3	FlowJo, LLC	https://www.flowjo.com/
Prism version 8.3.0	GraphPad Software, LLC	https://www.graphpad.com/
ImageJ 1.52p	Wayne Rasband NIH, USA	https://imagej.nih.gov/ij/
IMARIS version 9.1.2	Bitplane	https://imaris.oxinst.com/
Photoshop, CC2015	Adobe	https://www.adobe.com
Cell Ranger v3	10X Genomics	https://support.10xgenomics.com
R v3.6 & v3.4	The R Project	https://www.r-project.org
Docker v19	Docker	https://www.docker.com/
Singularity v2.6	Singularity	https://singularity.lbl.gov/
Snakemake v5.13	Snakemake	https://snakemake.readthedocs.io/en/stable/

RESOURCE AVAILABILITY

Lead Contact

Further information and requests for resources and reagents should be directed to Serge A. van de Pavert (vandepavert@ciml.univ-mrs.fr).

Materials Availability

This study did not generate new unique reagents.

Data and Code Availability

Sequencing data and codes were deposited in online databases. All RNA-sequencing data were deposited in the Gene Expression Omnibus public database as superseries under GSE153771. In-house-made code, original data, and corresponding docker images are available from the project github repository (https://github.com/CIML-bioinformatic/SPlab_BecomingLTi) both with a readme explaining the detailed procedure to reproduce the results.

EXPERIMENTAL MODEL AND SUBJECT DETAILS

Mice

Mice were maintained under specific pathogen free and a 12h light and dark cycle at an ambient temperature of 22°C in the animal facilities of the CIML (Marseille, France). Animals were housed in individually ventilated cages containing sterile quarter-inch corncob bedding for environmental enrichment. They were fed with irradiated standard pellet chow and reverse osmosis water. All experiments were performed according to the French ethics committee regulations. C57BL/6J and CD1 female and male mice were purchased from Charles River and Janvier Labs respectively. *RORγt*^{eGFP} mice were kindly provided by Gérard Eberl (Pasteur Institute, Paris, France) (Sparwasser et al., 2004). *Cdh5-CreERT2*$^{+/-}$ mice were kindly provided by Ralf Adams (Max Planck Institute for Molecular Biomedicine, Münster, Germany) (Sörensen et al., 2009). *Cxcr4-CreERT2*$^{+/-}$ (Werner et al., 2020) and the previously mentioned *Cdh5-CreERT2*$^{+/-}$ lines were crossed to homozygosity for the tdTomato reporter sequence using *Rosa*$^{tdTomato/\ tdTomato}$ (*Rosa*$^{tdT/tdT}$) (Madisen et al., 2010) mice and will be later referred to as *iCxcr4*^{tdT} and *iCdh5*^{tdT} respectively. Unless stated otherwise, female mice were used between 7 and 15 weeks of age and males were between 8 and 20 weeks of age. Analyzed embryos and adult mice included both females and males.

METHOD DETAILS

Timed pregnancies and Tamoxifen administration

For fatemapping of Lymphoid Tissue inducer (LTi) cells, *iCdh5*^{tdT} and *iCxcr4*^{tdT} male mice were crossed with C57BL/6J females. For induction of reporter recombination in the offspring, pregnant females were administered intraperitoneally 1.2mg of

4-hydroxytamoxifen (4OHT – Sigma T176) and 0.6mg of progesterone (Sigma P0130) at different embryonic stages (from E7.5 to E10.5). For adult fatemapping experiments, pups were delivered by C section and cross fostered with lactating CD1 females. For lymph node (LN) formation analysis, EdU experiment and bulk sequencing, male *RORγt*^{eGFP} mice were crossed with C57BL/6J female mice. For single cell sequencing, C57BL/6J male mice were crossed with C57BL/6J females. Mice were mated overnight, and the day of vaginal plug detection was marked as E0.5. Littermate embryos that were scored younger upon isolation were discarded from analysis.

Flow-cytometry

Embryos

iCxcr4^{tdT} embryos pulsed with 4OHT at E8.5 and collected at E9.5 were isolated. Embryos were carefully separated from the yolk sac and both tissues were analyzed for expression of Cxcr4 by tdTomato by flow-cytometry in endothelial cells stained with CD31 (Ebioscience 46-0311-80). Tissues were gently digested using liberase TM and DNaseI enzymes (Sigma-Aldrich 5401127001 and 11284932001 respectively) for 20min at 37°C under agitation as performed before (van de Pavert et al., 2014). After digestion cells were washed with RPMI 2% FBS (Sigma-Aldrich F7524), centrifugated (1250rpm at 4°C for 7 min) and resuspended. *RORγt*^{eGFP} embryos were collected between embryonic days E11.5-E14.5 and 4OHT pulsed *iCdh5*^{tdT} or *iCxcr4*^{tdT} embryos were collected at E13.5 or E16.5. Fetal livers (FL) were dissected from embryos and isolated for analysis of LTi cells. Brains of fate mapped embryos were isolated for analysis of tdTomato recombination in microglia. Limbs and all internal organs were removed to enrich for peripheral LN anlagen (except for E11.5 *RORγt*^{eGFP} embryos being too premature to remove all organs) and checked for LTi cells. This tissue is later mentioned as periphery. Tissues were gently digested as described above. Cells were blocked (15% normal mouse serum (Jackson Immunoresearch 015-000-120), in FACS buffer (HBSS 2% FBS)) for 15 min and subsequently stained for CD45 (BD biosciences 564279), F4/80 (BD biosciences 743280), CD11b (Ebioscience 11-0112-85), IL7Rα (Ebiocience 50-1271-80), CD4 (Biolegend BLE100422), $\alpha_4\beta_7$ (BD biosciences 740892) diluted in FACS buffer for 30min on ice. Cells were washed with FACS buffer and resuspended in Sytox Blue (Invitrogen s34857) diluted in FACS buffer after centrifugation (1250rpm at 4°C for 7 min). The liver of a few pulsed *iCdh5*^{tdT} embryos at E8.5 or E10.5 collected at E13.5 were stained for hematopoietic stem cells (HSC) progenitors using CD45, CD3e (Ebioscience 53-0031-82), CD19 (Ebioscience 11-0193-82), B220 (Ebioscience 53-0452-82), TER-119 (Ebioscience 11-5921-82), Ly6G (Ebioscience 11-5931-82), CD11b (BD biosciences 562128), CD117 (BD biosciences 563146), CD48 (BD biosciences 740687), F4/80 (Biolegend BLE123141), CD150 (Biolegend BLE115914), Sca1 (Ebioscience 17-5981-82) and zombie UV (Biolegend BLE423108). The staining of dead cells with zombie UV was performed for another 30 min after the antibody staining in protein free HBSS right after washing the cells. Cells were subsequently washed and resuspended in FACS buffer.

Adult mice

4OHT *iCdh5*^{tdT} mice pulsed at E8.5 or E10.5 were sacrificed between 7 and 9 weeks of age. Blood samples were drawn from the retro-orbital vein prior to sacrifice and subjected to red blood lysis prior to staining using RBC lysis buffer (eBioscience 00-4333-57). Brain, bone marrow, spleen, gut, cervical (C), mandibular (Md), mesenteric (M), axillary (Ax), brachial (Br) and inguinal lymph nodes (IngLN) were collected. The three latter mentioned LNs were pooled and referred to as AxBrIngLN on the graphs. Soft tissues including spleens, LNs and bone marrows (after the cells have been flushed from the bones) were gently digested as described previously. Red blood cell lysis was also performed on spleen and bone marrow samples prior to staining. Brains were prepared using the brain dissociation kit from Miltenyi (Miltenyi Biotec 130-107-677). Guts were prepared as described previously (Rankin et al., 2016). Briefly, small intestine was harvested and Peyer patches were removed as well as all the fat and faces. After cutting it longitudinally, 2-3cm long fragments were cut and placed in PBS. Pieces were then incubated for 30 min at 37°C under agitation (200rpm) in 20mL buffer A (HEPES 1M (GIBCO 15630-80), EDTA (Invitrogen 15576-028) 0.5M, 10% FBS in PBS). EDTA was washed 4 times with PBS and scissor minced pieces were incubated for 55 min at 37°C under agitation (200rpm) in 20mL buffer B (HEPES 1M, 10% FBS, 6000UI Collagenase (Sigma-Aldrich C2139) in RPMI). Remaining aggregates were mechanically disrupted using a syringe and cells were filtered over a 70μm cell strainer and washed with RMPI 10% FBS. After centrifugation (1500rpm at room temperature (RT) for 10 min), cells were resuspended in 5mL 100% Percoll (Sigma-Aldrich GE17-0891-02) and placed at the bottom of 5mL of 40% Percoll. Cells were centrifuged for 20 min without break (2100rpm at RT) and middle ring cells were harvested and washed with RPMI 10% FBS. Spleen, gut and LN samples were stained for CD45, CD11b (BD biosciences 563015), F4/80, CD3e (Ebiosciences 47-0031-80), CD19 (BD biosciences 562956), CD8a (BD biosciences 560776), Ly6G (Biolegend BLE127633), TCRβ (BD biosciences 563221), IL7Rα, $\alpha_4\beta_7$, CD4 and zombie UV. Blood samples were stained for CD45 (Ebiosciences 25-0451-82), CD3e, CD19, CD11b and Zombie UV. Bone marrows were stained for HSC progenitors as described previously. Brain samples were stained for CD45, CD11b, CD115 (Biolegend BLE135524), F4/80 and Sytox Blue. Samples were acquired on the LSRFortessa-X20 (BD Biosciences) cytometer and data were analyzed using FlowJo (version 10, LLC) software.

Immunofluorescence

4OHT pulsed *iCdh5*^{tdT} or *iCxcr4*^{tdT} embryos were collected at E13.5. Embryos were fixed by immersion in 4% paraformaldehyde (PFA - Electron Microscopy Science, ref 15714) for 30 min at RT, subsequently cryoprotected with 10% sucrose (Sigma-Aldrich S9378) and 30% sucrose in PBS overnight, frozen in OCT and 20μm cryosections were cut. Sections were first dehydrated in acetone (Carlo Erba chemicals 301505) for 10 min and after rehydratation in PBS, they were blocked (15% normal donkey serum (NDS, Jackson Immunoresearch 017-000-121), 2% BSA (ID bio 1000-70) in PBS) for 15 min and incubated with rat anti-CD4 (clone GK1.5,

eBioscience 14-0041-82) antibody diluted in EBSS 1% Triton X-100 2% BSA for 1h at RT. Sections were washed with PBS and incubated with donkey anti-rat Alexa Fluor 488 (ThermoFisher A-21208) for 45 min at RT, washed with PBS and mounted with Mowiol 4-88 (Calbiochem 475904) plus 1,4-diazabicyclo[2.2.2]octane (Sigma-Aldrich D27802) mounting solution. Images were acquired using Zeiss LSM 780 and 880 confocal laser scanning microscopes and analyzed using Fiji software.

Whole mount preparation and analysis

E11.5, E12.5, E13.5 or E14.5 *RORγt*^{eGFP} embryos were fixed in 0.4% PFA overnight at 4°C and subsequently placed in blocking medium (PBS-MT (1% skim milk, 0.4% Triton X-100 in PBS), 5% NDS) for three days. Embryos were incubated with anti-GFP (AVES, GFP-1020) and rat anti-CD4 in PBS-MT + 3% NDS for 7 nights and after washing with PBS + 0.2% Triton X-100 incubated with donkey anti-chicken Cy3 (Jackson Immunoresearch 703-166-155) and donkey anti-rat Alexa 647 (Jackson Immunoresearch 712-605-153) and βIII-tubulin Alexa 488 (Biolegend, 801203) in PBS-MT + 3% NMS for another 7 nights. Embryos were first washed with PBS + 0.2% Triton X-100 and dehydrated using methanol (Carlo Erba chemicals 412383) series (20%, 40%, 60%, 80% and 100% 1h each and 100% ON) and cleared using a 1:1 mixture of methanol and BABB (2:1 benzyl alcohol (Honeywell 108006) / benzyl benzoate (Acros organics 105862500)) for 8h. Clearing was completed by incubating embryos in BABB until acquisition. Embryos were acquired using the light sheet Ultramicroscope version II (LaVision BioTec).

EdU proliferation assay

Dams carrying *RORγt*^{eGFP} embryos were injected 2h prior isolation with 100μg/g of body weight EdU (Life technologies, C10646). Embryos were collected at E13.5 and FL and periphery were prepared as described before. Cells were first stained for CD45, F4/80, IL7Rα, $\alpha_4\beta_7$ and zombie UV. Then cells were fixed and permeabilized to stain for intracellular EdU following the protocol of the Click-it Plus EdU Flow-cytometry Assay Kit (Life technologies, C10646). Cells were subsequently analyzed by Flow-cytometry.

Next generation sequencing

For the bulk RNA sequencing, *RORγt*^{eGFP} E13.5 embryos were isolated and both FL or the embryonic periphery, enriched for peripheral LN anlagen and thus without thymus, gut or other organs were dissociated using the above-mentioned protocol. CD45$^+$ cells were enriched using CD45 magnetic microbeads (Miltenyi Biotec 130052301) on the autoMACS Pro separator. A lineage cocktail was used for removing possible T, B, dendritic cells and macrophages (CD3e (BD biosciences 562286), CD19 (BD biosciences 562291), CD8a (BD biosciences 562283), Ly6G (BD biosciences 562700), F4/80 (BD biosciences 565613)). Cells were subsequently stained and the common lymphoid progenitor (CLP) (alive Lin$^-$CD45$^+$IL7Rα$^+$$\alpha_4\beta_7^-$RORγt$^-$CD4$^-$), LTi progenitor (alive Lin$^-$CD45$^+$IL7Rα$^+$$\alpha_4\beta_7^+$RORγt$^-$CD4$^-$), LTi$_0$ (alive Lin$^-$CD45$^+$IL7Rα$^+$$\alpha_4\beta_7^+$RORγt$^+$CD4$^-$) and LTi$_4$ (alive Lin$^-$CD45$^+$IL7Rα$^+$$\alpha_4\beta_7^+$RORγt$^+$CD4$^+$) cells were sort-purified using the BD FACS ARIA III sorter. RNA was isolated using a RNA purification kit (Norgen Biotek Corp. 51800) and the quality and concentration of the RNA was determined with the bioanalyzer using RNA 6000 pico kit (Agilent 5067-1513) and Qubit fluorometer (ThermoFisher) using the Qubit dsDNA HS Assay Kit (ThermoFisher Q32854). Only those samples with a RIN value above 8 were used for subsequent library preparation. Samples were pre-amplified with the SMART-Seq v4 Ultra Low Input RNA Kit (Clontech). Libraries were generated with sample barcode and molecular indexing, the latter being used in order to provide an absolute digital measurement of gene expression levels. Sequencing was performed using a NextSeq 500, in 2 runs of 14 muLTiPlexed samples. NextSeq 500 data were demuLTiPlexed individually per sample. Furthermore, the raw fastq files were processed to trim the molecular barcodes, the end of reads depending on quality, and the potential remaining illumina adapters. A sequencing Quality Control (QC) step was run twice on the fastq file: before and after the trimming of the reads. Afterward, alignments were performed using STAR versus GRCm38 ensemble transcriptome resulting in a BAM which was qualified by Qualimap RNaseq. Detection and elimination of duplicated reads were done using MarkDuplicates. Finally, one table count by run was obtained using FeatureCount. Bioinformatics analysis were done in R using house made scripts. Normalization of counts and detection of differentially expressed genes was done using DEseq2 R package, PCA was done using the ade4 R package.

For the single cell sequencing C57BL/6J E13.5 and E14.5 embryonic peripheries and FL were collected and cell suspension were prepared as mentioned above. CD45$^+$ cells were enriched using CD45 magnetic microbeads on the autoMACS Pro separator. Cells were subsequently stained and alive CD45$^+$ F4/80$^-$ IL7Rα$^+$ LTi cells were sort-purified using the BD FACS ARIA III sorter. Sorted-purified cells were subsequently prepared for single-cell sequencing using the Chromium Single Cell 3′ kit from 10X genomics (v2 for periphery and v3 for FL (120267 and 1000092 respectively– California, USA) for the library preparation and the NextSeq 500/550 High Output Kit v2 (75 cycles) cartridges from Illumina for the sequencing. The quality and concentration of the cDNA was determined with the bioanalyzer using the High Sensitivity DNA Analysis Kit (Agilent 5067-4626) and Qubit fluorometer using the Qubit dsDNA HS Assay Kit. FASTQ raw files were processed using Cell Ranger software (v3, default parameters), which performs alignment, filtering, barcode counting and unique molecular identifier (UMI) counting. Reads were aligned to the mouse mm10 genome.

Quality control and cell filtering: Quality control (QC) was performed to remove poor quality cells thanks to in-house developed R scripts. Using Seurat R package CreateSeuratObject function, cells with less than 200 or more than 5000 (potential doublets) detected genes, cells with a too low or too high number of UMI (nUMI < median - 3MAD or nUMI > media + 3MAD) and cells with more than 40% mitochondrial gene expression (apoptotic cells) were removed. After quality control, for E13.5 FL 248 cells were taken out, leaving 10533 for analysis; for E13.5 periphery, 322 cells were taken out, leaving 4209 for analysis; for E14.5 FL, 678 cells were taken out, leaving 11410 for analysis; for E14.5 periphery 707 cells were taken out, leaving 4301 for analysis. Expression data were

normalized using the Seurat R package NormalizeData function (using logNormalize method and scale factor of 10000). Using PCA (see below), we observed a dependency in number of UMI in the first principal component. We centered and regressed the expression data from that factor using the Seurat R package ScaleData function (centering true and scaling false). Using Seurat clustering method, we observed several clusters expressing genes identified as contaminating cells.

Dimensionality reduction and clustering: we ran principal-components analysis (PCA) using the dudi.pca function from ade4 R package with data centering. We ran t-distributed stochastic neighbor embedding (t-SNE) implemented via Barnes-Hut approximations (bh-SNE), using the Rtsne function from Rtsne R package (perplexity = 30, and default option values). Clustering was done using two methods: (i) Seurat FindClusters based on PCA dimensionality reduction and the 10 first principal components; (ii) getKnnClusters function from Pagoda2 R package taking advantage of the Multilevel community detection method (Velocyto results; see below).

RNA velocity analysis

Single-cell RNA velocity analysis was done using the velocyto tool in two steps. First, we used the python implementation with the velocyto run CLI to produce a loom file with the model computation (see http://velocyto.org/velocyto.py/tutorial/cli.html#running-velocyto). Then, we used the velocyto and Pagoda2 R packages both with in-house developed scripts to produce further analysis from the obtained loom file, following Kharchenko Lab documentation (see http://pklab.med.harvard.edu/velocyto/notebooks/R/DG1.nb.html). Cell velocity flow was mapped on the t-SNE map produced at the previous steps using the show.velocity.on.embedding.cor function of the velocyto R package.

QUANTIFICATION AND STATISTICAL ANALYSIS

Quantification of LN formation

LN size was analyzed by counting the number of $CD4^+$ and GFP^+ cells at the right sides of the E11.5, E12.5, E13.5 or E14.5 *RORγt*^{eGFP} embryo using IMARIS software (version 9.1.2, Bitplane). CLN, MdLN, AxLN, BrLN, RenLN, IngLN and PopLN anlagen were analyzed.

Statistical analysis

Graphs, average values and standard deviation (SD) shown in all figures were calculated using Prism (version 8.3.0 GraphPad software) software. The number of individual experiments can be found in the legends of all the figures. Photoshop software (CC2015, Adobe) was used to generate figures.